CHALMERS
UNIVERSITY OF TECHNOLOGY

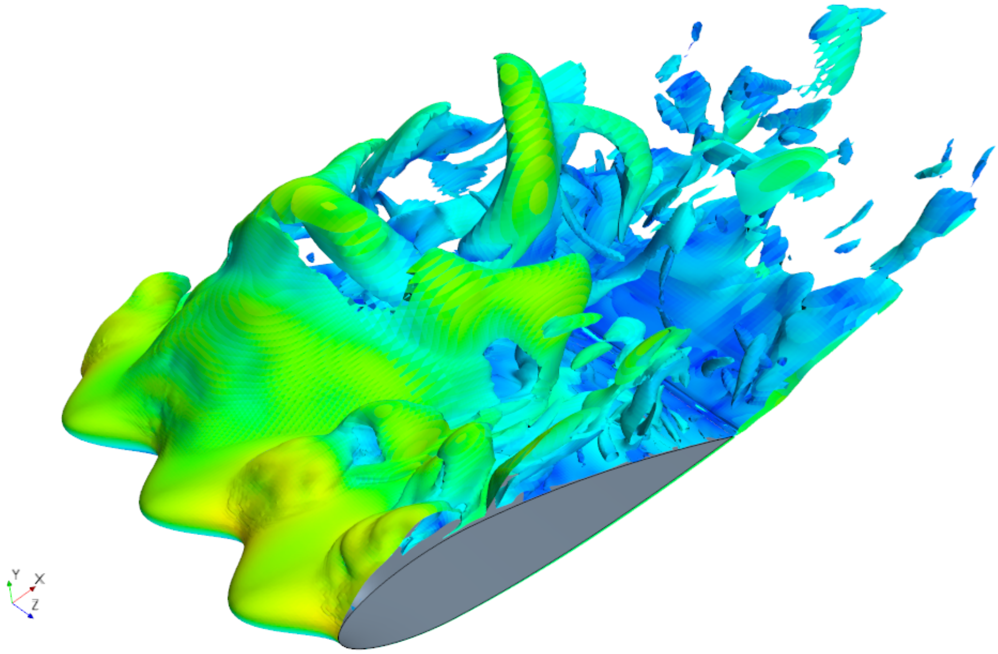

Application of a Humpback Whale Fin as a Rudder

Master's Thesis in Naval Architecture and Ocean Engineering

Jon-Asle Jansen
Jonatan Nilsson

Department of Mechanics and Maritime Sciences (M2)
CHALMERS UNIVERSITY OF TECHNOLOGY

Göteborg, Sweden 2017

MASTER'S THESIS 2017:06

Application of a Humpback Whale Fin as a Rudder

Jon-Asle Jansen
Jonatan Nilsson

Department of Mechanics and Marine Technology
CHALMERS UNIVERSITY OF TECHNOLOGY
Göteborg, Sweden 2017

Application of a Humpback Whale Fin as a Rudder
JON-ASLE JANSEN
JONATAN NILSSON

Supervisor: Arash Eslamdoost, Department of Mechanics and Maritime Sciences (M2)
Examiner: Arash Eslamdoost, Department of Mechanics and Maritime Sciences (M2)

Report No. X-17/273
Department of Mechanics and Maritime Sciences (M2)
Chalmers University of Technology
SE-412 96 Göteborg
Telephone +46 31 772 1000

Cover: Vorticity for foil A01N3 from current thesis.

Typeset in LaTeX
Printed by [Name of printing company]
Göteborg, Sweden 2017

Application of a Humpback Whale Fin as a Rudder
JON-ASLE JANSEN
JONATAN NILSSON
Department of Mechanics and Maritime Sciences (M2)
Chalmers University of Technology

Abstract

With ships growing larger and larger for each generation the need for better manoeuvrability increases. Previous studies have shown that redesigning the leading edge of the rudder will increase the manoeuvrability. A method for increased manoeuvrability is by mimicking the tubercles on the leading edge of the humpback whales flipper. The tubercles on the leading edge of the flipper will delay the separation, increasing the lift-to-drag ratio which in turn will yield a highly efficient rudder, making manoeuvring easier.

A parametric foil with the possibility to easily change the foils chord length, span width and thickness as well as the tubercles amplitude and wave length. Three different validation studies were conducted to confirm that it was possible to recreate the results from previous studies.

The investigation conducted by this thesis investigated 16 different foils with different characteristics to see which foil yielded the highest lift-to-drag ratio.

From the investigation of the foils it can be concluded that tubercles on the leading edge has a negative influence on the lift-to-drag ratio. Contradicting to our expectations was the foil that yielded the highest lift-to-drag ratio the foil with a flat-leading edge. However, further investigation of the foils at an angle of attack =0° needs to be conducted to examine the drag coefficient. If a foil, yields a high lift coefficient for high angles of attack while not increasing the drag for 0° it might still be beneficial to use that foil. This thesis is the first, to the authors knowledge, computational simulation to have as many wave lengths as 21.

Keywords: Tubercle, Humpback Whale, Bio-mimicking, Rudder, Foil, NACA, Manoeuvrability

Preface

This thesis has been conducted as the final work for the masters degree at the Department of Mechanics and Maritime Sciences (M2) at Chalmers University of Technology by Jon-Asle Jansen and Jonatan Nilsson.

We would like to thank our supervisor and examiner, Arash Eslamdoost, for all the help during the project. There would not be a thesis without his help.

We would also like to thank Nils Øyen at the Institute of Marine Research in Bergen. He has helped us trying to understand the reason for the tubercles on the leading edge of a humpback whale flipper. Furthermore he has put us in contact with other researchers around the globe.

We would also like to thank our fellow students Johannes Varosy and Hampus Martinsson that have helped and supported us during the thesis.

List of Abbreviations

- AoA - Angle of Attack
- C_D - Drag Coefficient
- C_L - Lift Coefficient
- Re - Reynolds Number
- C - Chord Length
- S - Span Width
- BC - Boundary Condition
- A - Foil Area
- RANS - Reynolds Average Navier-Stokes
- DES - Detached Eddy Simulation
- NACA - National Advisory Committee for Aeronautics
- NASA - National Aeronautics and Space Administration
- SST - Shear Stress Transport
- LES - Large Eddy Simulation
- CAD - Computer Aided Design
- CFD - Computional Fluid Dynamics

Contents

1 Introduction

Humans have a lot to learn from nature. We have in several cases exceeded nature in our designs, mostly because there are several technical designs that do not exist in nature.

Yet, when they do and we try to copy them, it often results in a poor version of natures own evolutionary design.

In later years, results have shown that if we use certain elements of designs shaped by evolution, it will improve our own designs. In the pioneering days of engineering it was nature itself that inspired engineers, for example the Wright brothers who invented the modern day wing that made it possible for humans to take to the skies.

Nature still inspires engineers to create new ideas and invent new technology. To be able to save planet Earth it will be even more important to look to our fellow inhabitants for inspiration.

Wind turbine have in many years been a green way of producing energy. In recent years, wind turbines have have grown larger and more powerful, which means that the distance between the wind turbines needs to increase. This creates further problem as wind farms require an enormous area.

To solve this, scientists have looked to schools of fish and the wake vortices produced by the fish. From this, engineers have created circular wind turbines that use the locations relative to each other to take advantage of air current between them. These new wind turbines have the potential to produce the same energy as traditional wind turbines, but with a decreased land area usage. (Amelia Hennighausen, 2017)

Everyone cannot invent such revolutionary designs, but to help our planet survive, young engineers of today can start with smaller problems and look to nature for guidance. An example could be to improve the efficiency of a rudder by mimicking the tubercles of the leading edge of humpback whales flipper. This could lead to both improved vessel navigation as well as better fuel economy.

1.1 Background

The unique thing about the humpback whale is that it relies on its superior maneuverability when catching prey. This makes the humpback whale truly unique among the members in the Rorqual family. The other whales in the Rorqual family (e.g. blue-, minke-, fin-) usually feed by lunge feeding, which means that the whale accelerates to a high velocity. When a high velocity has been reached the whale opens its mouth and engulfs its prey.

The Rorqual is a subspecies to the Baleen whale family containing eight different species. In the Baleen whales family it is generally more common, Rorquals excepted, with whales swimming slow, saving energy, through big patches of krill with the mouth open. The whales then filter the water out through the baleens (Fish and Battle, 1995).

The humpback whale uses its superior maneuverability in three different tactics to catch prey, upward lunge, inside loop and bubbling (Fish, Weber, et al., 2011). In the first tactic of feeding the humpback whale swims forward and then changes direction continuing by lunging upwards, between 30°-90° angle from the water surface, at speeds around 2.6 m/s forcing the prey towards the surface where it cannot escape.

In the *Inside loop* tactic the whale swims away from its prey, rolls 180° making a tight u-turn and then attacks its prey at full speed. This manoeuvre is performed within 1.5-2 body lengths of the whale (Fish and Battle, 1995).

The last way of catching pray is *Bubbling* (Fish, Weber, et al., 2011). While swimming around the patch of prey, the humpback whale blow out air from the blowhole. This creates a net of bubbles around the prey, catching them. While the whale is swimming towards the surface in a spiral shape, the net is tightening. In the end when the prey has gathered in a tight group the humpback whale pivot into the center and engulf the prey.

The reason for the humpback whales high maneuverability is the shape and size of the flippers. The flippers can be described as streamlined airfoils with a rounded leading edge and a slim pointy trailing edge, close to the shape of a symmetric NACA foil (Fish and Battle, 1995). In Figure 1 a standard NACA profile can be seen.

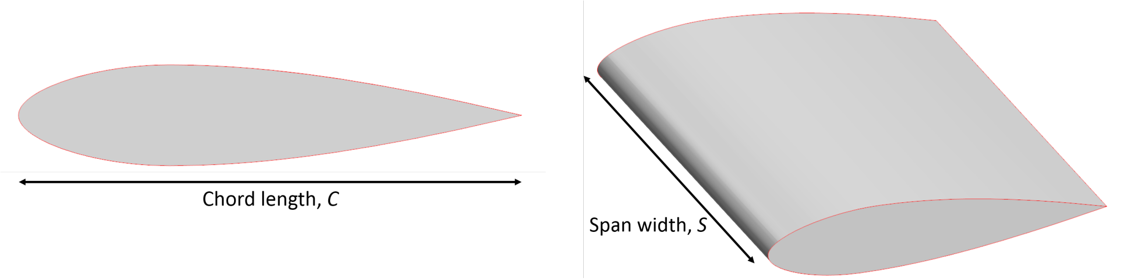

Figure 1: A standardized NACA foil.

The most unique feature of the humpback whale flipper is the tubercles on the leading edge. These tubercles are thought to be the main reasons for the humpback whales maneuverability. This is because the tubercles help to delay the separation from the boundary layer (Lohry et al., 2012). The tubercles are the humps on the leading edge of the flipper that can be seen in Figure 2.

Figure 2: A humpback whales flipper showing the tubercles on the leading edge.

Further important factors that impact the lift- and drag forces is the aspect ratio (Fish and Battle, 1995). It can be expressed as the length of a foil divided by the chord of the foil (Colin, 2015). A high aspect ratio will produce less induced drag. This is due to the wingtip having less area, which means that there will be less vortices, see Figure 3. At the same time, the maneuverability of a high aspect ratio foil will decrease (Colin, 2015). Another important factor is the planform of the flipper which is used to calculate the lift- and drag coefficient according to equation 1 and 2.

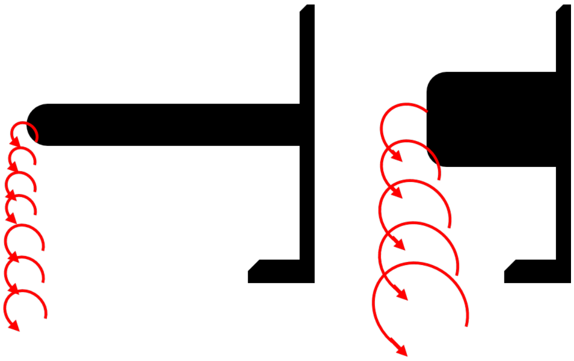

Figure 3: Vortices generated for two wings with different aspect ratio.

1.2 Objective

This Master's Thesis aims to examine the possibility of mimicking the shape of a humpback whale flipper on a rudder. The project will examine how the tubercles on the leading edge of a foil affect the lift-to-drag ratio generated by the foil. The main focus will be on finding a combination of amplitude and wave length that give the highest lift-to-drag ratio. To do this the flow physics of a foil with and without tubercles must be understood. Furthermore will a literature- and validation study be conducted during the project. As the results are dependent on factors such as time step, mesh sensitivity a study, showing the effect of these, will be conducted. The result will present plots of the lift-to-drag ratio for several foils as well as a conclusion of which combination of amplitude and wave length that give the highest result.

1.3 Limitations

The project will be conducted under the rules for a Master Thesis at Chalmers University of Technology. It will consist of 30 credits, equal to one semester of studies.

During the project only computer simulations will be conducted. To verify the accuracy of the data gathered in these simulations further real life measurements in a water- or wind tunnel needs to be performed. Moreover were no cost savings calculations conducted.

Further limitations are the cluster that will be used to do the simulations. During the project three different clusters, Glenn, Hebbe and Triolith will be used. For these cluster a specific amount of computational hours are granted. After these hours have been used there is a possibility to still use the cluster but the simulations will be deprioritized in the queue. There is also an finite number of nodes which mean that there is a risk for queues while still having computational hours to use.

1.4 Methodology Summary

A literature study will be conducted to get a good understanding of previous studies. With a wider knowledge of the area, a domain and a parametric foil is designed to be able to validate the previous studies. After the domain and foil has been validated, different foils will be investigated to see which combination of amplitude and wavelength produces the highest lift-to-drag ratio. Furthermore a time step dependency and mesh sensitivity study will be conducted.

2 Literature Study

Frank E. Fish was the first to investigate tubercles on the leading edge of a airfoil in 1995 (Fish and Battle, 1995). Since then he has conducted several studies on the tubercles including the effects of the tubercles on lift and drag and the geometry itself. According to Fish et al. (Fish and Murray, 2011), wind tunnel tests showed that an airfoil with leading edge tubercles improved maximum lift by 6%, increased the ultimate stall angle by 40%, and decreased drag by 32%. They were also able to see a decrease in noise emitted from the foil.

A physical change of the geometry of the foil is a passive method of enhancing the performance of a foil. The tubercles create vortices which travel down the chord length of the foil. The vortices are either co-rotating or counter rotating. Introducing these vortices to the boundary layer increases the velocity in the layers and thus increase the turbulent flow velocity. This means that the momentum exchange increase, which means that it takes more energy from the flow to separate and thus helps to delay the flow separation. (Hansen, 2012) (Bakker, 2006).

Fish et al. (Fish, Weber, et al., 2011) observed that implementing leading edge tubercles improved the lift significantly up to the post-stall regime, at 11°, while reducing drag. At the same time, the tubercles delayed stall for a flat foil from 11° to 17° for a foil with tubercles.

When stall occurred for a foil with tubercles it happened slow and graduate compared to a flat foil (Fish, Weber, et al., 2011) where the stall occurs sudden. It also showed that it had some increase in lift in the pre-stall regime, below 11°, but most important, no increase in drag. This resulted in a higher lift-to-drag ratio, both for mean and peak value. However, the most important improvement occurs in the post-stall regime.

In Figure 4 and Figure 5 the separation for a flat leading edge and tubercle leading edge is illustrated. For a flat leading edge foil the separation line is located at the same chord length position along for the entire spanwidth, see Figure 4. The separation begins near the trailing edge for low AoA and move towards the leading edge with an increase in angle of attack, AoA.

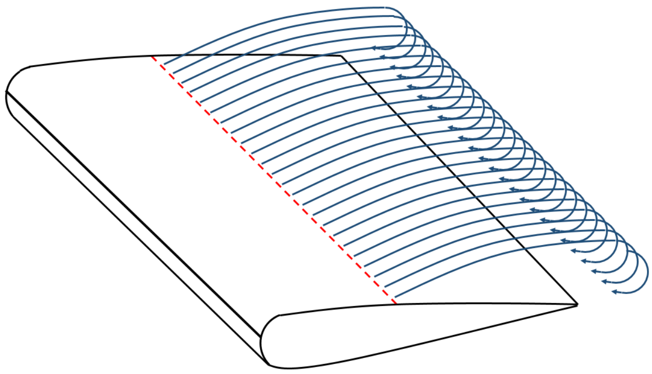

Figure 4: A foil without tubercles showing separation at same chord length position along entire span width.

The flow for the foil with tubercles on the leading edge is divided through the spanwidth (Hansen, 2012). As shown in Figure 5 the fluid separates almost at once in the trough i.e. between the tubercles. In contrast, behind the tubercles the flow does not separate. Which means that the foil is able to generate lift at higher AoA compared to a straight leading edge wing. This is also supported by earlier studies (Weber, Howle, et al., 2010) showing gradual stall and higher lift coefficients in post-stall regime.

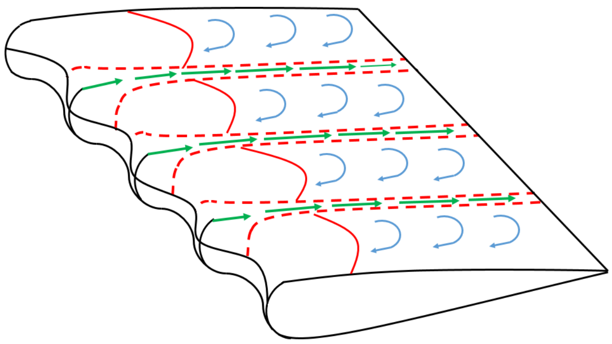

Figure 5: A foil with tubercles showing delayed separation at the tubercles.

Hansen (2012) writes, as Fish and Battle (1995) reported before, that there were no notable advantage of tubercles in the pre-stall regime. Instead the drag increased, giving a lower lift-to-drag ratio. In summary, the post-stall regime is where every study have showed significant improvements of the lift-to-drag ratio for leading edge tubercles.

2.0.1 Mail Correspondence

To get a more complete knowledge behind the theory and the evolution of the humpback whales tubercles, mail correspondence where started with a marine biologists with sea mammals as their special field.

Nils Øyen - Institute of Marine Research

Nils Øien is the leading expert at the Institute of Marine Research in Bergen, and explained that the tubercles may be for sensoric purposes only. That every tubercle had a straw of hair inside from when this ocean going mammal was a land based animal. Humankind does not know all that much about the humpback whale species and their evolution, but from what is common belief in the field of ontogeny, the study of an individual or art from the fertilisation of the egg to the organisms fully developed form, is that the organisms development as a fetus mirrored large parts of its evolutionary development. Øyen states that he has witnessed this exact theory in real life as the Minke whale has some of these tubercles, but as the fetus grows the tubercles disappear all together before it is born. The tubercles may not be for sensoric at all since all other baleen whales looses them before birth, but they have helped the humpback whale special adaption to hunt that type of prey they catch, but by Øyen's believes the combination of the high aspect-ratio of the front flippers and the low aspect-ratio for the tail is mainly what gives the humpback whale its acrobatic abilities. However Øyen do conclude that we do not know for certain why the humpback whale has the tubercles, but that the tubercles improve lift is for sure.

3 Theory

This chapter will explain how a airfoil generates lift and how tubercles on the leading edge will affect the lift-to-drag ratio. With the knowledge of how a airfoil works will the theory of a rudder be presented. After that a brief explanation of the turbulent flow models and Courant number is presented.

3.1 Foil Design

An airfoil is a wing profile where the foremost part is called the leading edge. The aft part of the foil is called trailing edge, see Figure 6 below. The top side of the foil is usually called the suction side and the bottom part pressure side.

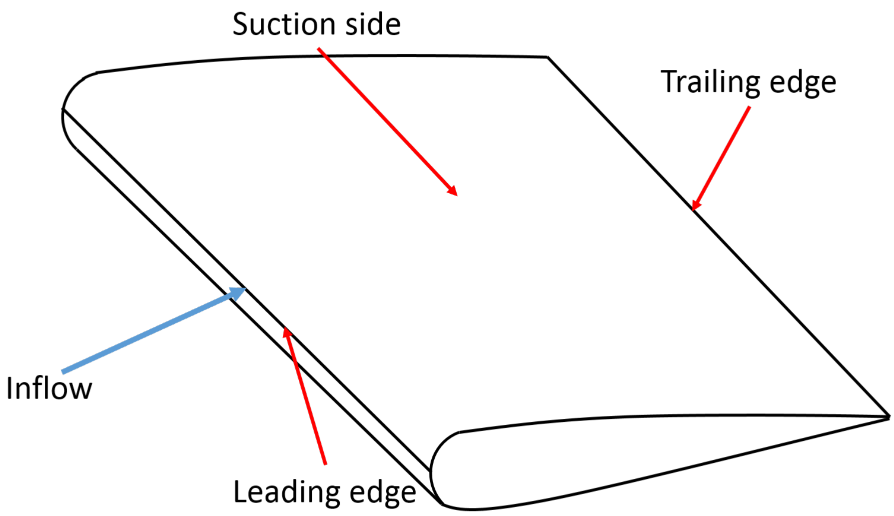

Figure 6: Principal sketch of a airfoil with the leading- and trailing edge as well as the suction side indicated.

An airfoil with an AoA, moving through a fluid will create a lift force perpendicular to the flow on the upper side of the foil. The flow will also generate a drag force parallel to the flow, usually consisting of friction and lift-induced drag. The reason for these forces are that the airfoil curves the streamlines as in Figure 7. This in turn induce a change in the pressure. On the suction surface the pressure will decrease while it increases on the pressure side of the foil (Babinsky, 2012).

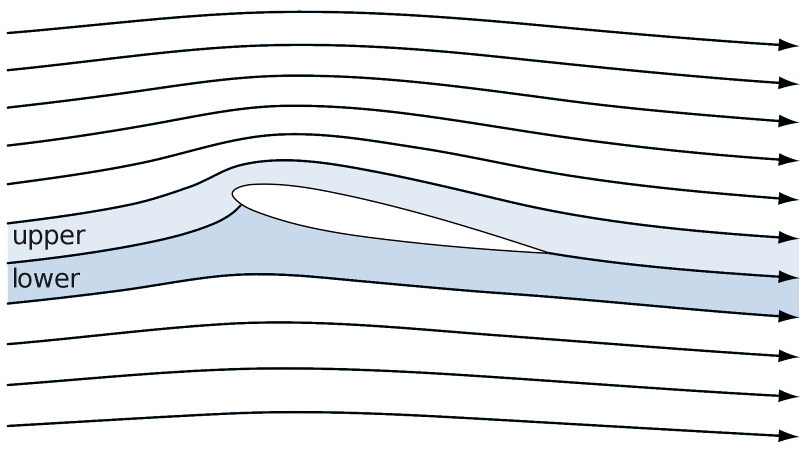

Figure 7: Foil with streamlines.

The lift and drag will increase with an increase of the AoA until it reaches the *critical angle of attack* where the lift force disappear. This phenomenon is called stall. The reason for stall is due to the turbulence created in the boundary layer by the flow separation. This will increase the pressure on the suction side of the foil, resulting in a rapid reduction of lift. At the same time the drag usually increase, lowering the lift-to-drag ratio even more.

A non-dimensional coefficient is introduced to be able to compare the foils with each other, regardless of the foil area and velocity. The lift coefficient is described as:

$$C_L = \frac{2F_L}{\rho U^2 A} \tag{1}$$

where F_L is the lift force, ρ is the density, U is the free stream velocity and A is the planform area, in this project seen as a square with the chord length C multiplied with the spanlength S. Even if the planform area changes with different AoA, the same planform area will be used to be able to compare the result more accurate. The drag is computed in a similar way:

$$C_D = \frac{2F_D}{\rho U^2 A} \tag{2}$$

where F_D is the drag force.

In this study the non-dimentional pressure coefficient C_P will also be used to compare and validate different foils and tubercle designs.

$$C_P = \frac{p - p_\infty}{\frac{1}{2}\rho V_\infty^2} \tag{3}$$

Where p is is the static pressure at the point at which pressure coefficient is being evaluated, p_∞ is is the static pressure in the free stream, ρ_∞ is the free stream fluid density, V_∞ is the freestream velocity of the fluid.

3.2 Rudder Theory

To turn the ship an angle of attack is induced to the rudder. When an angle of attack is introduced to the rudder, for example making the rudder turn to starboard, a lift force is then obtained towards port side of the ship (Jay, 2016). The rudder force will create a moment around the center of gravity, as in Figure 8. This moment however is not nearly enough to be able to turn the entire ship (Soumya, 2016).

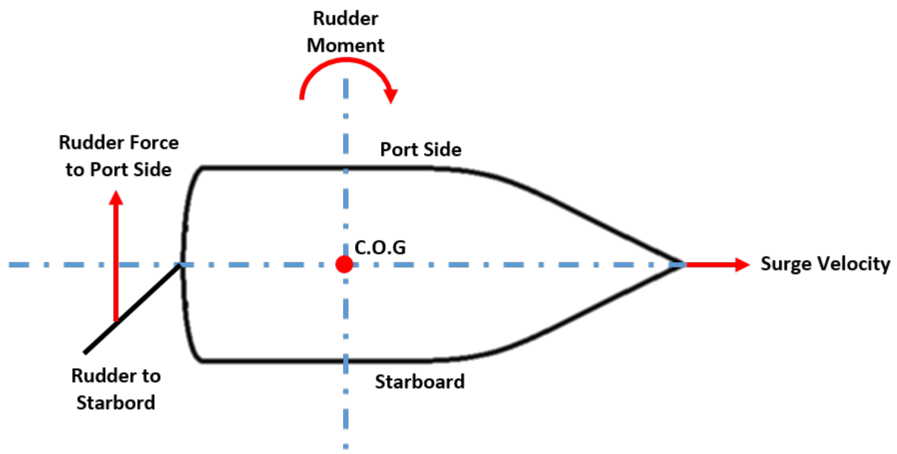

Figure 8: The rudder will induce a rudder force, perpendicular to the direction of the ship, that will induce a rudder moment around the center of gravity.

Instead the rudder moment around the center of gravity changes the orientation of the ship, inducing a small drift angle, as in Figure 9. The velocity of the ship is still in the same direction as in Figure 8 but the orientation of the ship is different due to the drift angle. With the drift angle is not only a surge velocity component obtained. Instead is a sway velocity component obtained as well. This makes it obvious that there is a sway towards port side when conducting a starboard turn (Soumya, 2016).

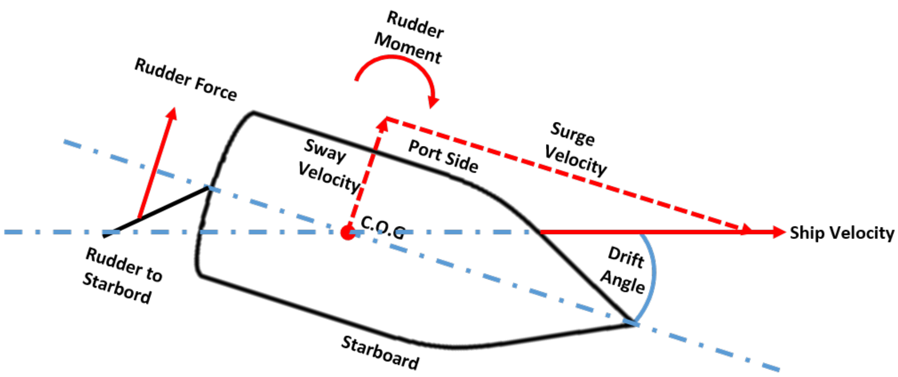

Figure 9: A drift angle is introduced from the rudder moment, changing the orientation but not the direction of the ship.

When the ship sway towards port the ship exerts a force on the water and the water exerts a force on the hull of the ship due to the inherent inertia of the water. This inertia has the opposite direction from the sway velocity component. The inertia can be divided into to two different parts, inertia acting on the bow and inertia acting on the stern see Figure 10.

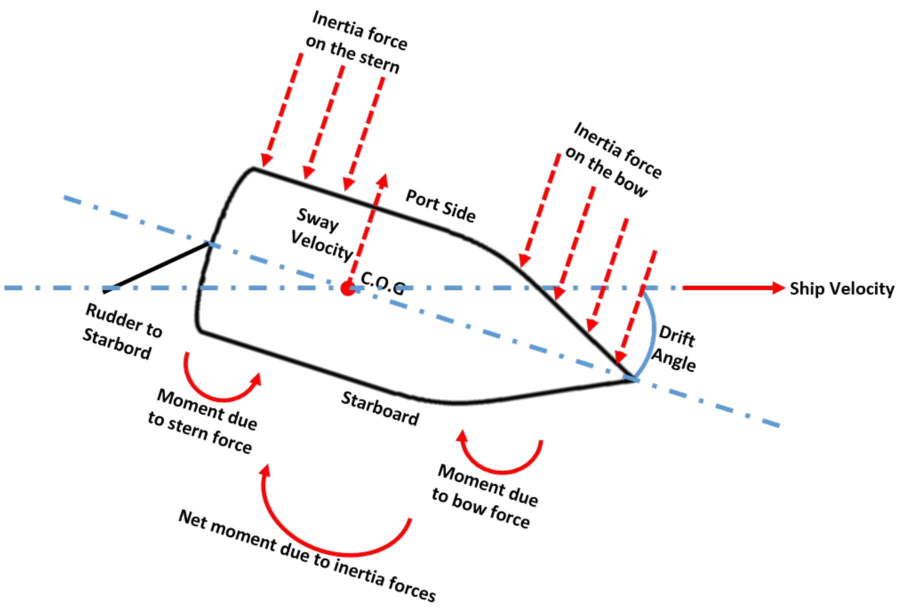

Figure 10: The net moment is clock-wise due to the inertia forces on the bow being dominating.

As can be seen in Figure 10 the inertia force on the stern will create a anti-clockwise moment around the center of gravity, turning the ship towards port side. Whereas the inertia force on the bow will create a clock-wise moment around the center of gravity, making the ship turn towards starboard. Because the design of the hull the force on the bow will be larger compared to the force on the stern making the clock-wise moment around the center of gravity dominating. As nature strives to get a equilibrium between the inertia force exerted by the water and the inertia force exerted by the hull the moment will be in the same magnitude as the displacement of the ship. This is the reason that the moment is great enough to be able to turn the ship (Soumya, 2016).

The efficiency of the rudder depends on several aspects but according to (Vacanti, 2005) the most critical are a low wetted surface, low frontal area and a high aspect ratio. Furthermore should the leading edge of the rudder be near to vertical. A swept leading edge will result in the planform rotating oblique to the water flow, working as a break and not a lifting surface, making turning impossible. This will become more evident the greater the sweep back angle is. More obvious is the importance of the area of the rudder (Jab, 2015) as well as the shape of the rudder. The rudder area should be around 1/60 to 1/70 of the immersed middle plane area of the ship (Soumya, 2016).

3.3 NACA Foil design

All foils tested in this thesis, as well in the three validation cases, are created by using the NACA-4DS curve tool in CAESES. It is a tool to help generate a generic four digit ***National Advisory Committee*** *for* ***Aeronautics*** airfoil. The airfoil design tool uses four parameters, chord length, thickness, camber and camber position.

For a NACA0020 foil the first digit,(0), indicates the amount of camber. The second digit, (0), indicates the position of the camber. Having a camber that is zero mean the foil is symmetric around the mid-line. The last two digits, (20), indicates the thickness as percentage of the chord length. For a NACA0020 this means the maximum thickness of a 1m long foil is 0.2m(Marzocca, 2017). The NACA foil is modelled in the XY-plane.

3.4 Tubercle Design

As mentioned before is the main reason for the humpback whale's maneuverability believed to be the tubercles along the flippers leading edge. Earlier studies have showed several beneficial effects such as an increase in lift at higher angles of attack and when it the critical angle of attack is reached, it does not stall sudden and abrupt but instead gradually. However, there are negative contributors as well.

The tubercles on the leading edge, x_{LE}, of a flipper can be described as a sinusoidal curve as:

$$x_{LE} = A\cos\left(\frac{2\pi}{\lambda}z\right) \tag{4}$$

where A is the amplitude, λ is the wavelength and z is the coordinate along the span. Another way of describing the sinusoidal curve is:

$$x_{LE} = A\cos\left(\frac{2\pi n}{S}z\right) \tag{5}$$

where n is the amount of humps on the leading edge of the foil and S is the spanwidth of the foil.

According to previous studies there are four major factors that affect the efficiency of the foil: Reynolds Number, Wave Length, Amplitude and Aspect Ratio. In the present study the effect of the aspect ratio will not be investigated. Instead focus will be on the affect of amplitude and wavelength.

Reynolds Number
Both Fish and Hansen (2012) writes in their reports about the importance of the Reynolds number and how it determines whether the tubercles are beneficial or not. Different studies have used different Reynolds number when examining the efficiency of tubercles on the leading edge. This means that there is a lot of data available, but since the foils that are used are not identical it is hard to determine how the Reynolds number affects the results.

For instance, Stanway (2008) writes that the lift-to-drag ratio will decrease for Reynolds number between 44,000 - 120,000 compared to a traditional leading edge.

Hansen (2012) on the other hand reports that a foil with tubercles, like the humpback whales flipper, decreased the tip vortex cavitation and increased the vorticity that delayed separation at a Reynolds number of 500 000.

After reading several studies, it seems that there are few to none studies or experiments that have been done on foils with tubercle leading edge at Reynolds number larger than 1 000 000.

Fish and Murray (2011) states that for a low aspect ratio rudder, the separation delay leads to an improved maximum AoA to 22° with Reynolds number of 200 000. However, they also states that when reaching higher Re numbers, the benefits diminished and the tubercles increased the onset cavitation.

Amplitude and Wave Length
There are different results for how important the wavelength is. According to Hansen (2012) the foils with the lowest value for tubercle amplitude and wavelength deliver the best results. But, according to Nierop et al. (2009) the wavelength had little to no influence on the result. However, in the wind tunnel tests, it did show a small dependence on wavelength.

A numerical optimization study was completed by Shi et al. (2016). In the study a conventional S814 airfoil, that can be seen in Figure 11, was compared to an S814 airfoil with tubercles on the leading edge. After an initial investigation an optimization of the amplitude, wave length and coverage of tubercles on the leading edge was conducted. It showed that the wavelength that had the best performance was a tubercle wave length of 0.5C, and tubercles amplitude of 0.1C. C meaning the Chord length. According to their result did the tubercles increase the lift-to-drag ratio with 32% at a post stall angle of 16°.

Figure 11: A S814 Airfoil used in the numerical optimization study

A further optimization, involving the coverage of tubercles changed the design even further. By testing 1/4, 1/2, 3/4 and the whole span length covered by tubercles. The best results was obtained with only 1/4 of the span length covered with tubercles. The lift coefficient and lift-to-drag ratio had a lower peak value. But for the C_L and lift-to-drag ratio in the pre-stall area and over a larger span of AoA the result were better. There was a slight increase in drag coefficient, but the lift-to-drag ratio still increased by 10%. The report concluded that the airfoil with 1/4 of tubercle coverage delivered the best results over a much larger span of angle of attack.

Application of tubercle leading edge

The literature review shows that this is a highly applicable technology. It needs more testing as the exact theory behind why the vortices behave as they do is unclear. To be able to control in which direction the vortices rotate may help improve the hydrodynamics properties even more.

There are several areas where wing like foils are used. They have already been mounted on wind turbines and can generate electricity at lower air speed as they now can increase the turbine blades angle of attack. Fans for air conditions have also been produced where they found that a 5 tubercle bladed fan was 20% more efficient and needed 25% less power do the same job as a 10 normal bladed fan (Fish and Murray, 2011).

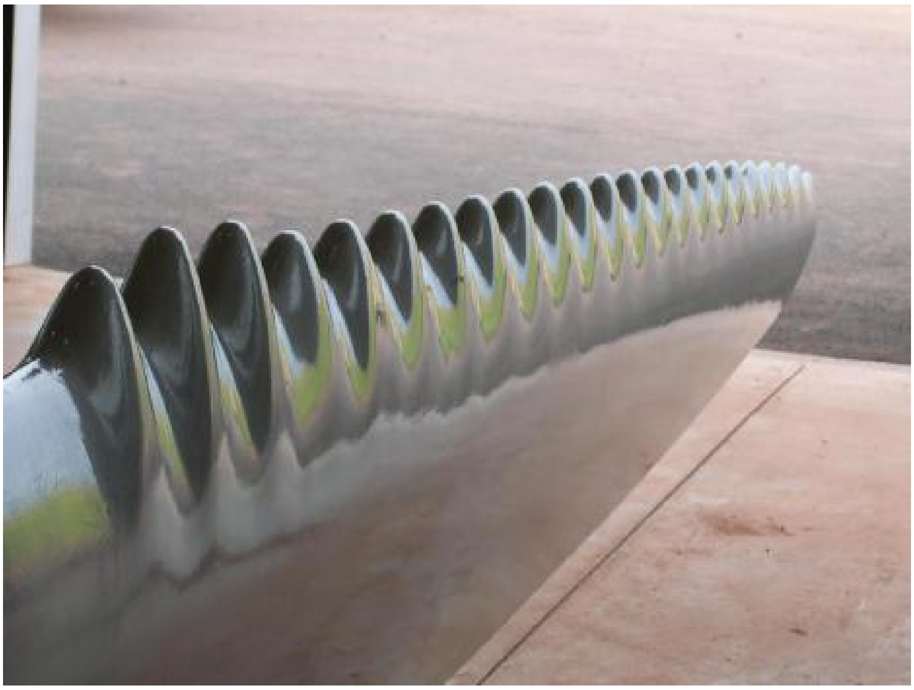

Figure 12: A wind turbine blade with tubercles on its leading edge.

3.5 Turbulent Flow Models

In this section are the turbulent flow models used in the simulations explained.

3.5.1 Reynolds Average Navier-Stokes

To model the turbulent flow Reynolds Average Navier-Stokes (RANS) is used. With RANS the flow will be decomposed into two different components, one fluctuating- and one mean component. By doing this an unknown term is obtained, called the Reynolds stress, $(\rho\overline{u_i'u_j'})$. The equations can then be evaluated by solving the Reynolds stress with a turbulent model. The RANS equation is described as:

$$\rho\bar{u}_j = \frac{\partial \bar{u}_i}{\partial x_j} = \rho\bar{f}_i + \frac{\partial}{\partial x_j}\left[-\bar{p}\delta_{ij} + \mu\left(\frac{\partial \bar{u}_i}{\partial x_j} + \frac{\partial \bar{u}_j}{\partial x_j}\right) - \rho\overline{u_i'u_j'}\right] \tag{6}$$

where $\bar{u}$ is the mean velocity, u' is the fluctuating velocity and f_i is a vector representing external forces.

3.5.1.1 Spalart-Allmaras model is developed especially for airfoils and wings, in particular for wall-bounded flows. It is a one-equation model which solves a transport equation for the kinematic eddy viscosity ν_T (Spalart and Allmaras, 1994).

3.5.1.2 SST K-Omega is the standard turbulence model employed in industry. It replaced the old industry standard k-ϵ model due to the k-ϵ only being accurate for fully developed turbulent flows as well as non-separating flows. The standard k-ω model is accurate in the near wall region while still giving accurate predictions of the flow separation from the foil. By combining the standard k-ω model for near wall treatment and the k-ϵ model away from the foil the combined SST k-ω model is obtained. This model will have near wall accuracy as well as away from the foil(Menter, 1994).

3.5.1.3 Detached Eddy Simulation (DES) is a combination of RANS solvers such as Spalart-Allmaras or SST k-ω with *Large Eddy Simulation* (LES) where the RANS is used in the near-wall regions and LES in the rest of the domain (Strelets, 2001). The LES model ignores the smallest length scales, making it a fast and cheap. However this makes the model unfit for the near-wall region where a lot of small scales are present and this is the reason for combining it with a model that is better for the near-wall region (Zhiyin, 2015).

3.5.2 Wall Treatment

Wall functions are not applicable for a foil with an angle of attack(Team, 2012). Instead it is suggested that the boundary layer is resolved all the way to the wall with an enhanced wall treatment such as a finer mesh close to the wall. This can be done by using *Prism Layer mesher* in STAR-CCM+. To do this the value of the first prism layer need to be calculated.

y^+ is a non-dimensional wall length that is often used to describe the distance from the wall. The reason for having a non-dimensional distance is that the information obtained at a dimensional distance does not say much about the flow, by using a non-dimensional distance the flow can be compared to other flows and the characteristics of the different boundary layer regions can be described more exact.

As can be seen in Figure 13, the flow has been divided into four different sublayers with different characteristics. *Viscous Sublayer* is the lowest layer, $y^+ < 5$. The second layer is the *Buffer Layer* for $5 \leq y^+ < 30$.

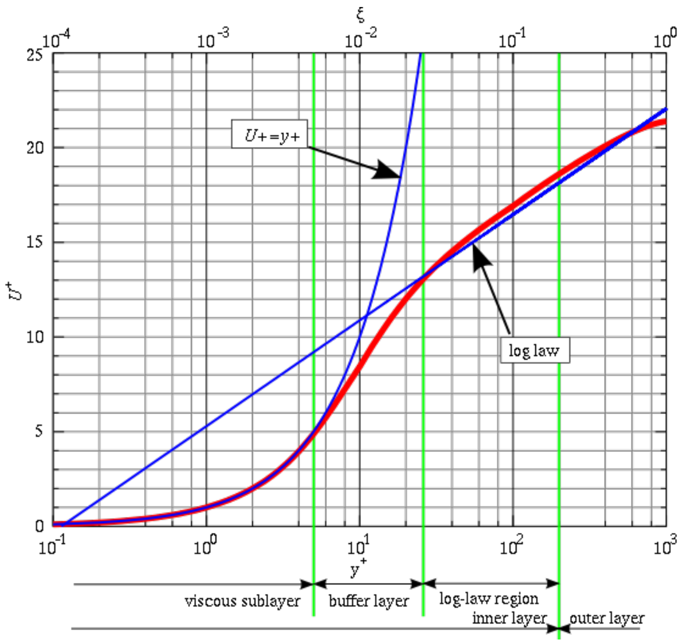

Figure 13: Law of the Wall curve, showing the different regions near the wall (Aokomoriuta, 2011)

For flows where there are a risk for separation it is important to use a a model that resolves all the way down to the viscous sub-layer, also known as the low-Re region. To resolve the laminar sub-layer when using a low Reynolds model the y^+ value should be around $y^+ = 1$. For further refinement near wall enhancement can be used but it is more often recommended to use a SST model such as $k - \omega$ (Team, 2013)

In order to estimate the the first prism-layer's height before the mesh generation, the following steps are taken. The Reynolds number is calculated from:

$$Re_x = \frac{\rho U_\infty L}{\mu}$$

where ρ is the density of the medium investigated, U_∞ is the undisturbed flow velocity, L is the chord length of the foil and μ is the dynamic viscosity of the medium investigated at a certain temperature. The skin friction can be estimated from the local skin friction equation of a turbulent flat plate, as follows:

$$C_f = \frac{0.026}{Re_x^{\frac{1}{7}}}$$

. From this the wall shear stress is calculated with the skin friction, density and velocity:

$$\tau_{wall} = \frac{C_f \rho U_\infty^2}{2}$$

The friction velocity can be described as:

$$U_{fric} = \sqrt{\frac{\tau_{wall}}{\rho}}$$

Having set $y^+ = 1$ and calculated the friction velocity, the height of the first cell can be described as(White, 2011).:

$$\Delta S = \frac{y^+ \mu}{U_{fric} \rho}$$

3.6 Courant Number

The Courant number can be described according to:

$$CFL = \frac{U \Delta t}{\Delta x} \tag{7}$$

where U is the free stream velocity, Δt is the time step and Δx the length of a cell. If the value of CFL is equal to 1 it means that a particle in the flow moves from one cell to the same position in the cell next to it in one time step. If the value is below 1 it is possible that the particle does not have the ability to cross the boundary into the next cell during one time step, giving two results from one cell. In contrast, having a high Courant number will mean that information from certain cells are lost due to the particle missing cells. Since the expression for the Courant number in equation 7 is linear it is possible to calculate a timestep close to 1 (Giraldo, 2006). In STAR-CCM+ it is possible to use Physical model called *Convective CFL Time Step Control* that let the user choose a target CFL and a minimum time step. The software will then automatically change the timestep to get the a proper CFL.

4 Methodology

The project is started by creating a parametric foil in CAESES©. The foil geometry is then transferred to STAR-CCM+ where the simulations will be conducted for different AoA. Furthermore the foils examined will be presented as well as a mesh sensitivity study and a time step dependency study.

4.1 CAD-Modelling in CAESES

CAESES© is a software used to create a parametric design of the foil which makes it easy to alter the important parameters. The important parameters on the foil is the foil length and thickness as well as the tubercles wavelength and amplitude. Using CAESES© allowed for several different foils to be created in a short period of time.

The tubercles are modelled according to equation 5 from Section 3.4. The equation is used in CAESES© to describe a *Fspline curve*, modelled in the XZ-plane.

To create the foil and the surface in CAESES©, the software uses a start- and end curve as well as an outline curve. The leading edge is used as start curve and the trailing edge as end curve. The surface will then be created from the leading edge to the trailing edge, following the outline of the NACA foil created.

The tubercles should have a smooth transition from the leading edge to the foils maximum profile thickness where the tubercles stops(Lohry et al., 2012). From the maximum thickness of the foil and backwards there should be no difference between a foil with tubercles on the leading edge and one without.

4.2 Simulations in STAR-CCM+

To be able to execute the simulations in STAR-CCM+ a domain needs to be designed. The domain is a block with the foil inside, which can be seen in Figure 14. When designing the domain size it is important to remember two things. To design it large enough in so that the boundary walls do not interfere on the results, and small enough that the computation time is kept down. For these reasons the domain size is set to $8C$ before and $20C$ after the foil as well as $10C$ above and below of the foil. In Figure 14 the boundaries are enumerated. For the inflow boundary, 1, *Velocity Inlet* boundary condition is used. For the outflow boundary, number 2 in the figure, a *Pressure Outlet* boundary condition is used. The third boundary condition is valid for the top and bottom boundary of the domain where the boundary condition is set to symmetry. The remaining two boundaries on each side of the foil, number 4, an interface between the two is generated. It is then set to have periodic boundary condition.

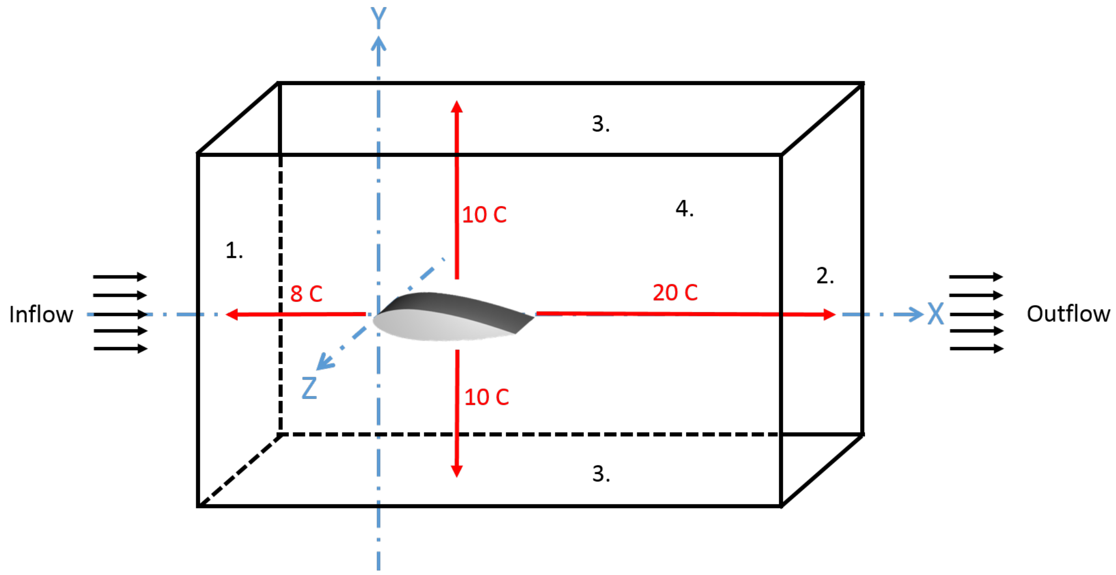

Figure 14: 3D view of the domain and the placement of the foil within it.

4.2.1 Mesh Modelling

After that a domain with boundaries has been created a mesh for the domain needs to be applied to get cells where the simulation can be conducted. The mesh is created by using the *Trimmer* model that use a template mesh, usually a hexahedral mesh, and trim it to fit the surface. The *Surface Remesher* model is then used to retriangulate the surface. Close to the foil there is need for mesh refinement according to Section 3.5.2 and therefore the *Prism Layer Mesher* is chosen.

In the *Prism Layer Mesher* the stretching model is set to *Wall Thickness* to be able to change the distance from the foil to the first mesh layer, according to section 3.5.2. Moreover the *Do proximity refinement* and *Retain geometric features* for *Surface remesher* is disabled. Finally *Do proximity refinement* is disabled and *Do mesh alignment* is enabled for *Trimmer*.

As can be seen in Figure 15 and 16, there are five different regions in the volume mesh with four different mesh sizes. The reason for this is to increase the computational accuracy at key areas of the domain. The rest of the domain has a coarser mesh to decrease simulation time. The mesh size is thus smaller the closer the region is to the foil. The position of the finer mesh can be seen in Figure 15 and the values of the mesh is displayed in Table 1.

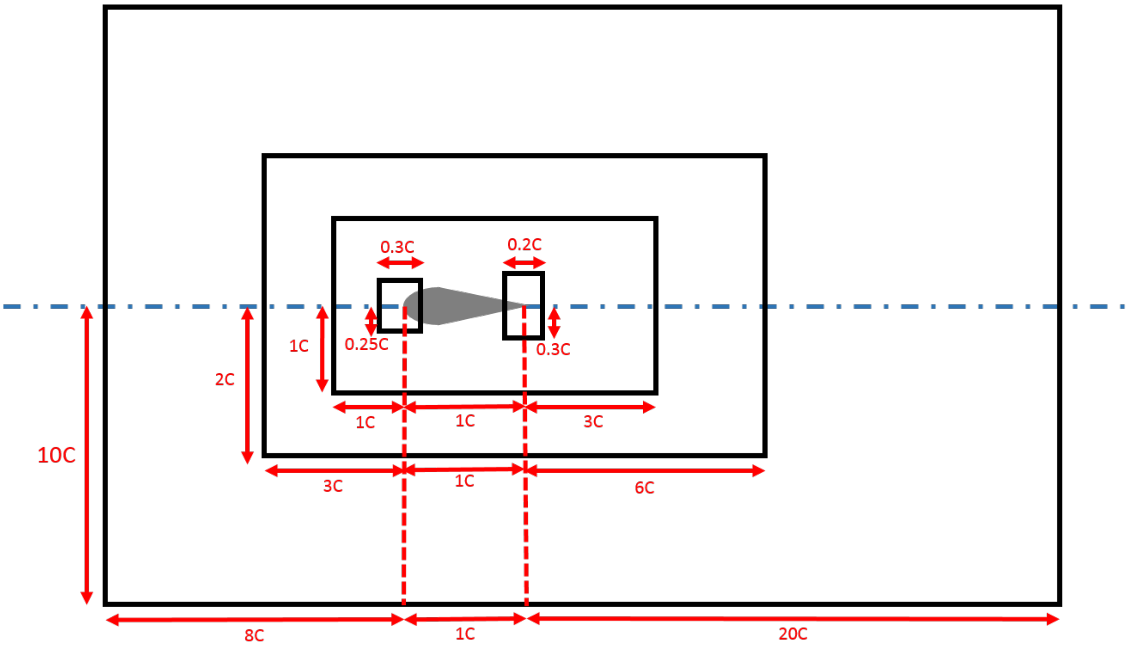

Figure 15: The domain with the different volumetric blocks displayed.

Table 1: Size of the different volume meshes and the custom foil mesh, *[% of base size].

Mesh	Size [m]	Mesh Size [%*]	Mesh Size [m]
Base Size	0.04	100	0.04
Volume mesh	2.8*2.0*0.05	100	0.04
Volumetric mesh 1	0.9*0.4*0.05	20	0.008
Volumetric mesh 2	0.4*0.2*0.05	5	0.002
Volumetric mesh 3	0.03*0.05*0.05	2	0.0008
Volumetric mesh 4	0.02*0.06*0.05	2	0.0008
Foil Region custom mesh		1	0.0004

As stated in section 3.5.2 there is a need for a finer mesh around the foil. This is achieved by using prism layers around the foil as in Figure 16. Depending on the simulation, the number, thickness and the distance from foil to first prism layer differ. For all simulation $y^+ = 1$ is used. In this report this will be presented in connection with the different simulations.

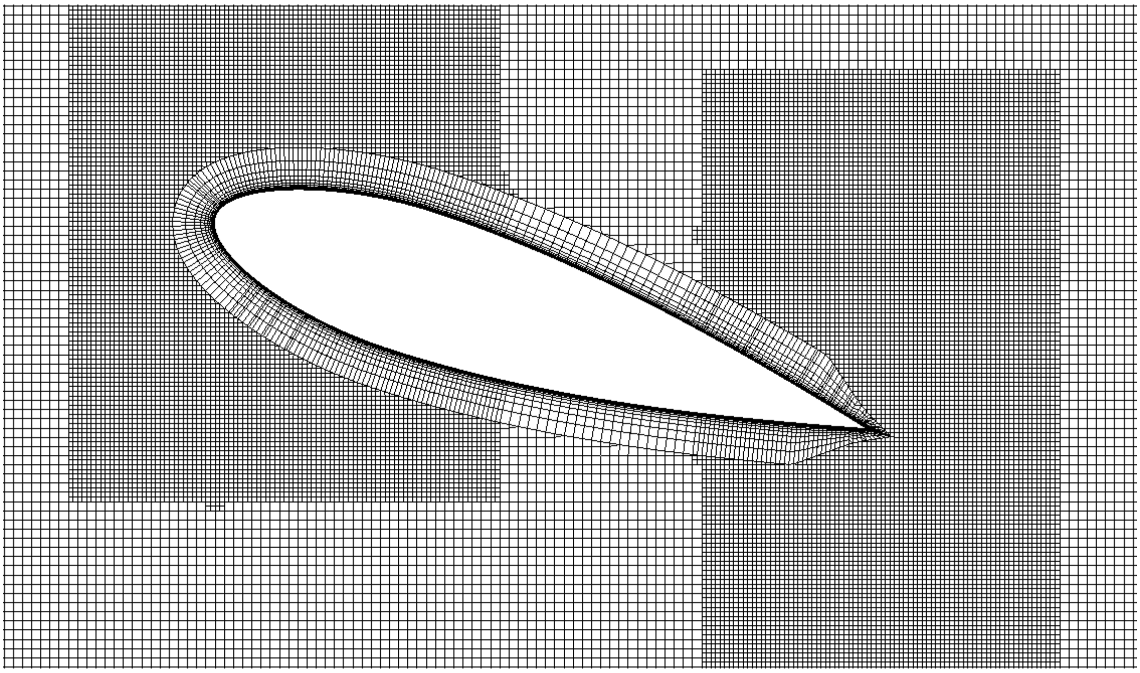

Figure 16: Prism Layers around the foil.

Below in Figure 17 the mesh generated on the surface of the foil can be seen. To get a good representation of the shape of the foil the surface mesh has been assigned a custom surface size.

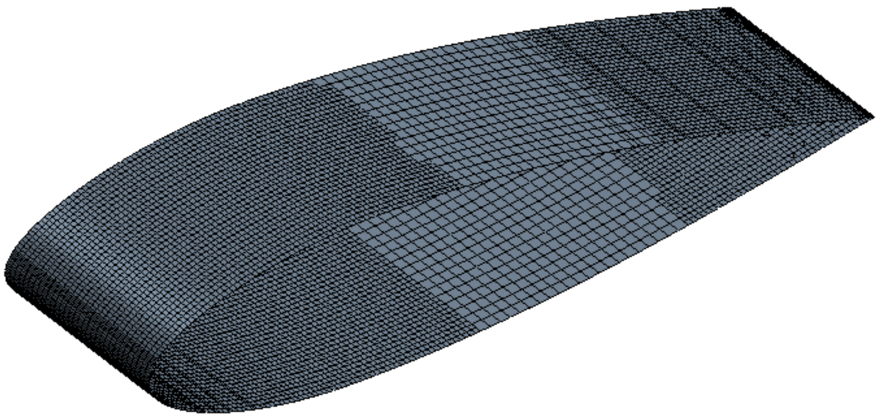

Figure 17: Surface mesh at the foil.

4.2.2 Physics Modelling

After designing a domain and applying the mesh the physics need to be applied. The flow inside the domain will be able to move in three dimensions and be able to be turbulent. The method for calculating the lift- and drag-coefficient and the treatment of the near wall region need to be decided. In STAR-CCM+ this is done by using *Physics models* and the models that are used can be found as a list in Appendix A.1. The following is a description of the the solvers used in current thesis's simulations. Other solvers during the validation study have been replaced, as it is stated in each validation study case in section 5.

Segregated flow solver is used since the flow is considered to be incompressible. It takes less computational time than Coupled flow, as it solves the velocity and pressure equations separate, rather than coupled. Coupled flow solver could be better at higher flow velocities such as supersonic. At these high velocities, high density fluctuations often occur which coupled flow solver calculates better. In the current case the velocity is significantly lower. For segregated flow a flow particle needs to flow trough the domain several times to get an accurate solution. Segregated flow solver is thus selected in current slow velocity flow case.(CCM+, 2017)

The *Implicit scheme for unsteady flow* is used. The implicit scheme means that the calculation done for every iteration is not only dependent on the previous time level N, where N is the number of iterations, but also on the current time level, $N + 1$. This is a more time consuming calculation as it requires greater computer resources. However, one can due to this use larger time intervals than that of using a Explicit scheme. This also increases the accuracy of the result.(Science, 2017)

The calculations are done using a turbulent flow model which is described in section 3.5.

The foil will generate vorticity and therefore it is important to get a good prediction of the flow in the near wall region. This is done by using the *All y^+ Wall Treatment* model that use the low-y^+ wall treatment for the fine mesh and the high-y^+ wall treatment for the coarse meshes. The low-y^+ wall treatment solves the viscous sublayer, $y^+ \leq 5$ whereas the high-y^+ uses a wall function to model the near wall region.

4.2.3 Main Particulars for simulation

The main particulars for the simulations can be seen in Table 2 below. A table for each validation case, Chapter 5, is presented in the associated section.

Table 2: Design parameters for simulation.

Parameter	Abriviations	Value
Chord Length	C	0.1 [m]
Span Width	S	0.08 [m]
Freestream Density	ρ	998 $[\frac{kg}{m^3}]$
Freestream Velocity	U	4.4525 $[\frac{m}{s}]$
Dynamic Viscosity	μ	8.871E-4$[kgm^{-1}s^{-1}]$
Reynolds number	Re	500 000
Desired y^+	y^+	1
Prism Layers	n	55
Prism Layer Thickness	L	0.005 [m]
Thickness of near wall Prism Layer	ΔS	4.4732E-6 [m]

4.3 Foils for investigation

The foils investigated were chosen from combining conclusions from several previous studies. The parametric foil created in CAESES was modified into 16 different foils, see Table 3, that were investigated for four different AoA; 6°, 12°, 16° and 20°. The four AoA were chosen due to a combination of computational time and previous studies of foils with leading edge tubercles. When testing 16 different designs, the number of AoA could not be more than four to be able to finish within this thesis's given time aspect. However, 6°, 12°, 16° and 20° provides a good overview of the overall performance of the airfoils.

The first 9 foil's investigation was performed to understand the amplitude and wavelength effects on the lift-to-drag ratio. The design was based on foil 4878 (Lohry et al., 2012) but the wavelength was decreased to fit more tubercles on the leading edge. Furthermore were the amplituded varied from 0.005m to 0.01m.

According to Hansen (2012) the highest lift-to-drag ratio was obtained for the foils with the lowest amplitude. For foil 10-12 the influence of the lower amplitudes are investigated. To get well defined tubercles, the wavelength was decreased as well.

As good results for the original 4878 foil (Lohry et al., 2012) was obtained further investigation of this foil was conducted with foil 13-15. For foil 4878 the amplitude is close to 0.008m. The foils were designed by combining this foil with the conclusion from Hansen Hansen (2012) claiming that thetubercles with low amplitudes gave the best result.

Table 3: Main particulars for the different foils investigated

N^o	Foil	Amplitude [m]	Wave Length [m]	Tubercles [n]
1	A005N3	0.005	0.0267	3
2	A005N4	0.005	0.0200	4
3	A005N5	0.005	0.0160	5
4	A0075N3	0.0075	0.0267	3
5	A0075N4	0.0075	0.0200	4
6	A0075N5	0.0075	0.0160	5
7	A01N3	0.01	0.0267	3
8	A01N4	0.01	0.0200	4
9	A01N5	0.01	0.0160	5
10	A001N9	0.001	0.0089	9
11	A002N9	0.002	0.0089	9
12	A002N15	0.002	0.0053	15
13	A002N2	0.002	0.0400	2
14	A004N2	0.004	0.0400	2
15	A008N2	0.008	0.0400	2
16	A005N21	0.005	0.0038	21

4.4 Mesh sensitivity study

Four different meshes (M1, M2, M3, M4) were generated for a mesh sensitivity study where the effect of the grid refinement was evaluated. All of the simulations were conducted with a time step of 0.001s for the exact same domain and foil. The A002N15 foil was used for evaluation. This foil has an amplitude of 0.02m and 15 tubercles giving quite small tubercles which need a refined mesh to represent the surface of the foil. For foils with larger tubercles there is less need for mesh refinement on the foil.

Table 4: Comparison of lift- and drag coefficient for different amount of cells

Foil	AoA [°]	Cell count	C_L	C_D	$\frac{C_L}{C_D}$
A002N15 M1	12	4303124	0.729	0.089	8.191
A002N15 M2	12	8593727	0.785	0.087	9.022
A002N15 M3	12	10314601	0.730	0.094	7.766
A002N15 M4	12	26564005	0.915	0.060	15.164

The result from the study can be seen in Table 4 where it is clear that the mesh refinement effects the result. The highest lift-to-drag ratio is obtained for the finest mesh, M4. However, the second finest mesh, M3, yields a lower lift-to-drag ratio than the coarser mesh of M1 and M2. When using as fine mesh as mesh M4 it was found that the time step needed to get a reasonable Courant number, was too low to use in practise as explained in section 4.5. A finer mesh requires a lower time step to get a good Courant number as explained in Section 3.6. However, the simulation with mesh M4 was not run with a low enough time step and it is highly plausible to be incorrect. The end decision was due to consideration of computational efficiency and mesh M2 is therefore used. This mesh yields the second highest lift-to-drag ratio while not requiring too much computational power.

4.5 Time step sensitivity study

A time step sensitivity study was conducted to see how the lift-and drag coefficients were effected by the time step used. Initially a time step of $t = 0.0001s$ was used, close to the value of $t = 0.0003s$ used by Rostamzadeh (Rostamzadeh et al., 2017). The time step $t = 0.0001s$ was used to as get a Courant number closer to 1, as the time step used by Rostamzadeh is not optimal in views of Courant numbers. Higher values of the time step were then investigated to see the possibility of increasing the speed of the simulation.

With the *Courant Number* the required time step could be calculated giving a timestep of $t = 2.5E - 7s$ for a Courant number of 1 according to Section 3.6. Simulations with this time step was conducted where the simulation ran for 250600 iterations, with the physical time at the end being 0.019s. This meaning that a time step that small is practiclt impossible to use for this thesis' time resources. As mentioned in Section 4.2.2 the *Segregated Flow* model need time for a particle to travel through the domain several times. Thus it is important that the simulation is aloud to run for a least 4-5 seconds of physical time. The lift-and drag coefficients obtained from the study can be seen in Table 5.

Table 5: Comparison of lift- and drag coefficient for different time step.

Foil	AoA [°]	Time Step [s]	C_L	C_D	$\frac{C_L}{C_D}$
NACA0020	6	0.001	0.202	0.020	10.100
NACA0020	6	0.0001	0.295	0.025	11.800
NACA0020	12	0.001	0.440	0.046	9.565
NACA0020	12	0.0001	0.979	0.185	5.292
NACA0020	16	0.001	0.707	0.096	7.365
NACA0020	16	0.0001	0.820	0.110	7.455
NACA0020	20	0.001	0.893	0.168	5.315
NACA0020	20	0.0001	0.977	0.184	5.310
A002N15	12	0.01	0.987	0.076	12.986
A002N15	12	0.001	0.785	0.087	9.022
A002N15	12	0.0001	0.952	0.071	13.600

From the study it is obvious that the time step influences the lift-to-drag ratio a great deal.

5 Validation of previous studies

To be able to base the present simulations on former studies it is important to confirm that the results from those studies can be recreated. To do this, three different cases were examined and recreated. The three cases were given the names Foil 4878, Foil A14W52.5 and Foil Weber et al. The foils and their domains were recreated and different combination of physical models were examined. This is to get confirmation from three different cases to what extent current CFD simulations are correct.

The **Foil 4878** study is called *Characterisation and Design of Tubercle Leading-Edge* and is written by Mark W. Lohry, David Clifton and Luigi Martinelli (Lohry et al., 2012). The study is using a standard NACA0020-foil with a redesigned leading edge. The name 4878 is given due to the number of tubercles, the wavelength of the tubercles and the span width according to equation 5.

The second study **A14W52.5** is called *A numerical investigation into the effects of Reynolds number on the flow mechanism induced by a tubercled leading edge.* It is written by Nikan Rostamzadeh, Richard M. Kelso and Bassam Dally (Rostamzadeh et al., 2017). The study uses a NACA-0021 foil which is very similar to NACA0020, but with a bit higher maximum height of the profile. The name given comes from the foil dimensions were A14 is the amplitude of 14mm and W52.5 is the wavelength of 52.5mm.

The last validation study is the **Weber et al.**. The study is called *Computational Evaluation of the Performance of lifting Surfaces with Leading-Edge Protuberances* by Paul W. Weber, Laurens E. Howle, Mark M. Murray and David S. Miklosovic. This is the study that differs the most, containing a foil that looks like a real humpback whale flipper. The name of the validation study comes from one of the authors, Paul W. Weber.

5.1 Foil 4878

The first validation study (Lohry et al., 2012) a NACA0020 foil. The tubercles on the leading egde are designed according to:

$$x_{LE} = 0.04\cos(4.878\pi z)$$

which gives the foil in Figure 18a. To see how the results differ between a foil with tubercles and a flat foil, a version of the same foil without the tubercles is also created 18b.

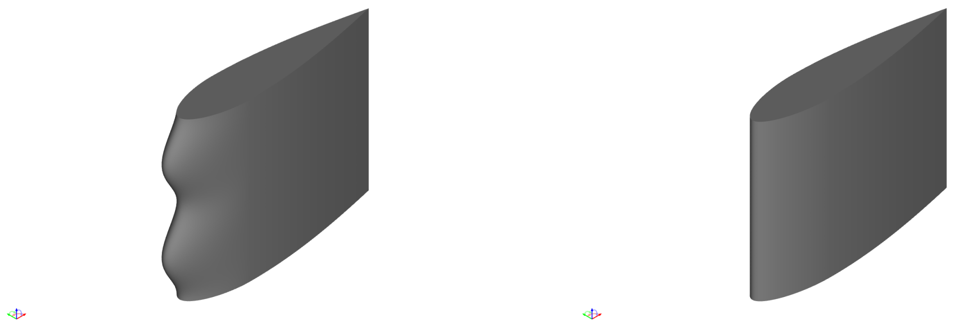

(a) Foil with tubercle design on leading-edge.

(b) Foil with standard design on leading-edge.

Figure 18: Foil with tubercle design from Characterisation and Design of Tubercle Leading-Edge study.

The input data that have been used for the 4878 validation simulation can be seen in table 6.

Table 6: Main particulars for the 4878 Validation Simulation.

Parameter	Abbreviations	Value
Chord Length	C	0.1 [m]
Span Width	S	0.08 [m]
Area	A	0.008 [m^2]
Freestream Density	ρ	998 [$\frac{kg}{m^3}$]
Freestream Velocity	U	4.4525 [$\frac{m}{s}$]
Dynamic Viscosity	μ	8.871E-4 [$\frac{kg}{ms}$]
Reynolds number	Re	500,000
Desired y^+	y^+	1
Prism Layers	N	55
Prism Layer Thickness	L	0.005 [m]
Thickness of near wall Prism Layer	ΔS	4.4732E-6 m [m]

Lift- and drag plots

The CFD analysis results provided in the article are listed below in table 7, which are the results that the validation simulation will be validated against.

Table 7: The lift- and drag coefficients for different angles (Lohry et al., 2012).

AoA [deg]	C_L	C_D
0	0	0.021
2	0.133	0.023
4	0.270	0.027
6	0.400	0.037
8	0.649	0.052
15	0.932	0.129
16	0.889	0.148
17	0.748	0.162

The first attempts at to run CFD simulation resulted in an asymmetric flow. The boundary condition was thus altered to create an interface between the two boundary sides. It could then be set to periodic along with detached eddies. This allows for a more realistic simulation of the oscillations happening. The asymmetric flow was only visible at high angles of attack where the flow separation occurs early. The original time step of 0.001 seconds was decreased to 0.00001 seconds to capture the unsteady flow structures more accurately. At later stages the time step was increased to 0.001 seconds, as the difference in end results was minimal.

The article states the cell count of the mesh to be 6.5 million compared to present study with 6.3 million cells. The 200 000 cells in difference did not effect the end results notably. At 16° and higher, STAR-CCM+ used 100 000+ iterations and 16 physical seconds to converge and get a stable result. From AoA from around 12° takes longer time to converge than for lower AoA.

The data from from Lorey et Al (Lohry et al., 2012) and Weber experimental data (Fish, Weber, et al., 2011) are plotted together with present study CFD results in Figure 19.

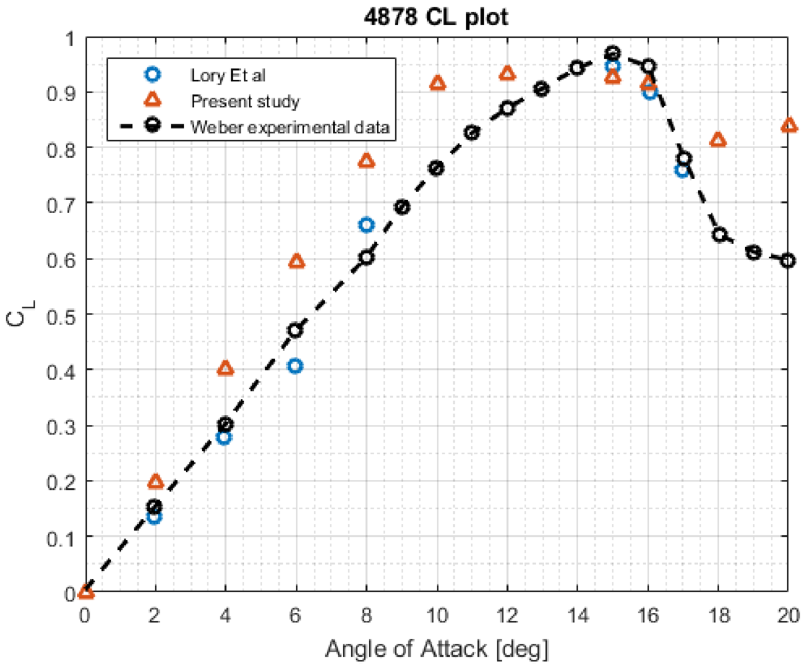

Figure 19: Results for C_L from the 4878 validation foil CFD simulation.

For the drag coefficient in Figure 20 the validation simulation as can be seen in Figure 19 there is quite a good match between the experimental data and current CFD simulations. However, the lift coefficient for the simulated validation study differs and give higher results in general. The largest difference observed from experimental data to current CFD simulations are at AoA = 20. There are also some difference from current CFD simulations to the experimental data at AoA = 8°to 15°. These differences could be due to the computational difficulty that occurs at fast oscillating flow. The For the pre-stall angles the differences are smaller, but the results are in general higher compared to the experimental data. These angles however, is not tested by the Lory et al, for unknown reasons.

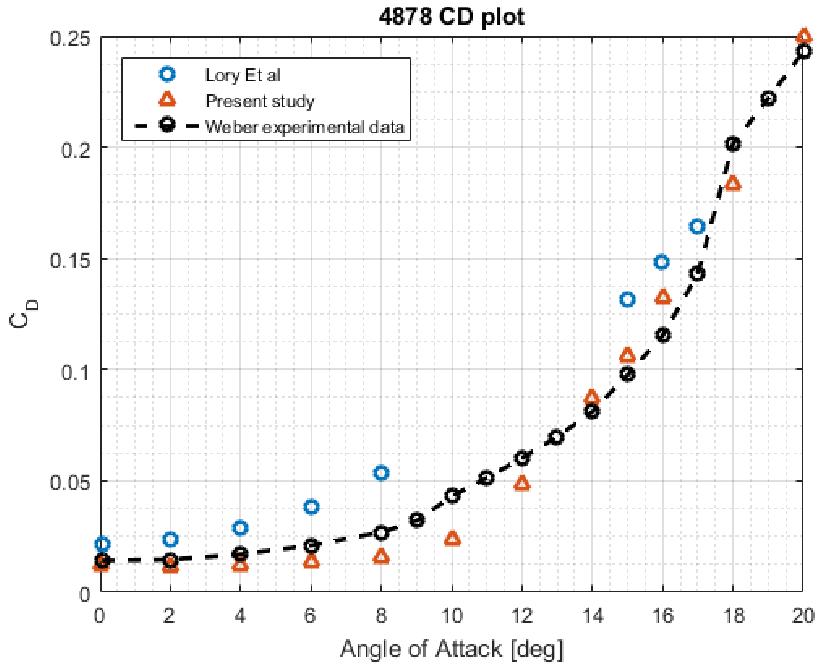

Figure 20: Results for C_D from the 4878 validation foil CFD simulation.

The drag coefficient in Figure 20, the current CFD results are close to the experimental data. One can also observe that current CFD results are more accurate to the experimental data than Lory et al. results.

Pressure Coefficient plot

The pressure coefficients for an angle of attack 8°, 15° and 20° presented in Figures 21, 22 and 23. In the figures are the pressure coefficient for foil 4878 at peak and trough as well as a foil with a flat leading edge presented. The pressure distribution is shown against the X position along the chord length C.

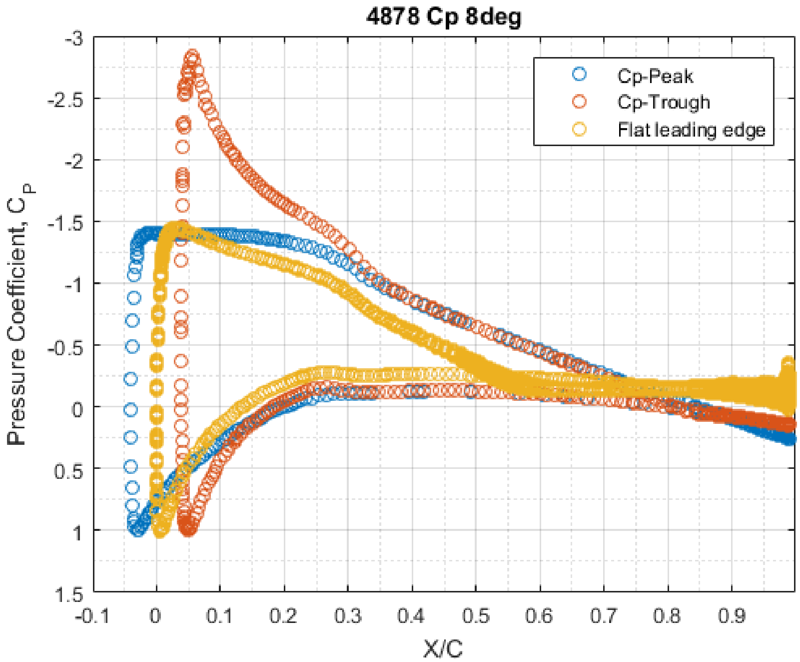

Figure 21: Pressure coefficient for both peak and trough for AoA=8°.

In figure 21 the AoA is 8°. This is a fairly low angle at which there are little difference in lift and drag coefficients when comparing flat leading edge and turbercled leading edge. Here the peak value for tubercle maximum and flat leading edge are very similar. However, the pressure increases quicker and at 0.55C it is almost zero for the flat leading edge foil. At this point the tubercle peak C_P and trough C_P is at -0.5 and are decreasing slowly at the same rate. As discussed previously in section 3.4, the vortices generated by the tubercles helps maintain flow velocity at the suction side.

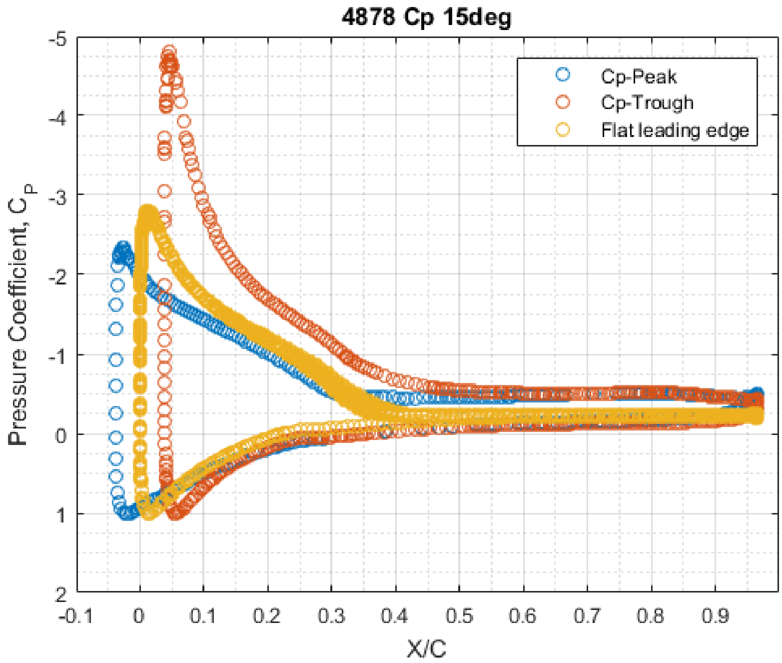

Figure 22: Pressure coefficient for both peak and trough for AoA=15°.

When looking at figure 22 and 23, one can notice the same pattern as in figure 21 at 8°. Only here, the peak value of C_P for the flat leading edge have a small increase at 15°. At 20° however, the flat leading edge C_P has a large increase while both tubercle peak and trough show similar results for both 15° and 20° angles.

At 15° the tubercle foil maintains a lower pressure further back on the suction side compared to the leading edge as seen for 8°. Resulting in a higher lift coefficient for the tubercle foil.

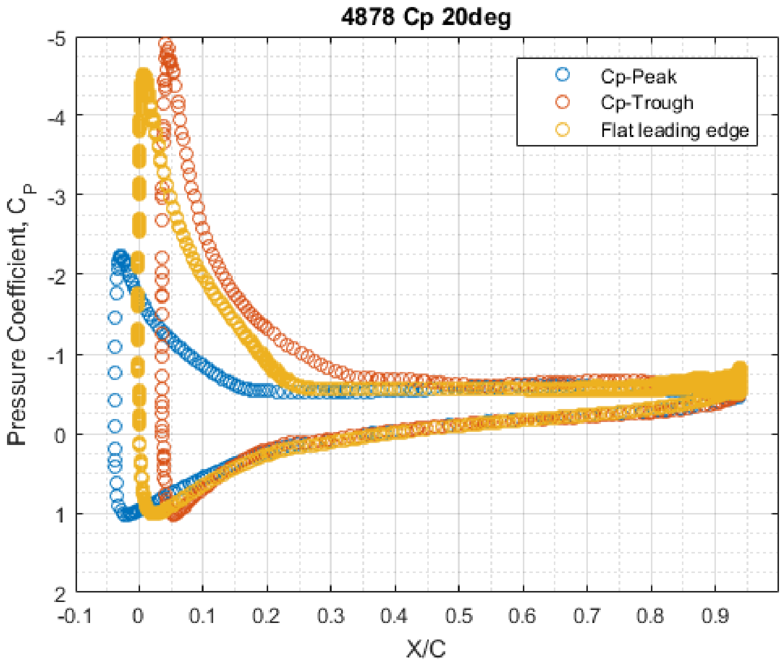

Figure 23: Pressure coefficient for both peak and trough for AoA=20°.

When looking more closely on the pressure side on both foils, one can see that the pressure coefficient on the flat leading edge is actually a bit lower. The calculated C_P at the pressure side at AoA of 20° is very similar, but it is lower for the flat leading edge at 8° and 15°. This means that the drag coefficient at 8° and 15° is lower compared to the tubercle foil. This will of course effect the total lift-to-drag ratio.

Limiting streamlines

In Figure 24 are the limiting streamlines plotted on the surface of the foil. These figures clearly show where the flow separates and the turbulence begin as well as the effects of the tubercles on the leading edge. Comparing the foils for an angle of attack of 8 ° it can be seen that the flow in Figure 24a separates at roughly the same position. But for the tubercle foil, Figure 24b, the flow stays attached almost until the trailing edge where it separates behind the tubercle trough.

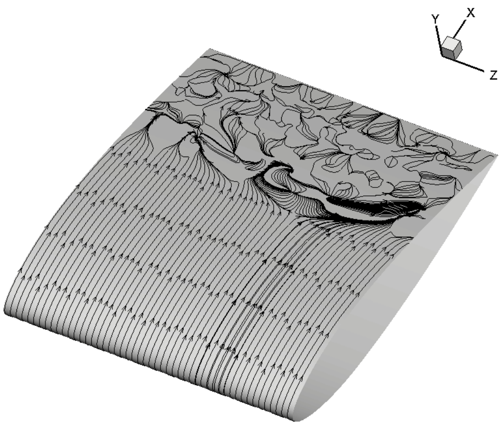

(a) AoA=8°.

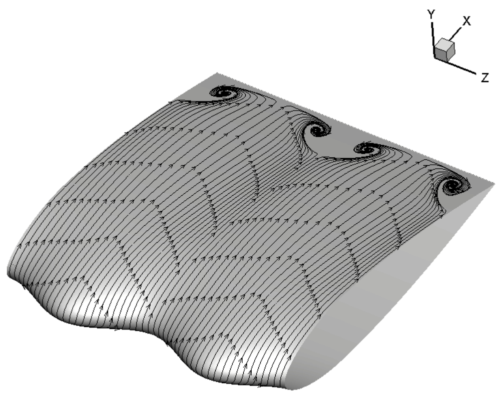

(b) AoA=8°.

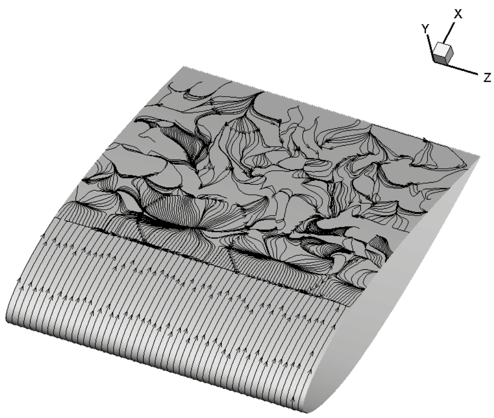

(c) AoA=15°.

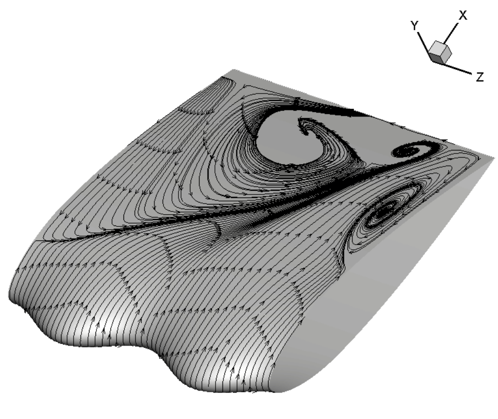

(d) AoA=15°.

Figure 24: Limiting streamlines for foil 4878 and a flat leading edge foil.

In Figure 24c where the foil is at 15°the limiting streamline show a very similar result as for the flat leading edge at 8°. It separates at the same chord length across the foils span width. However, looking at the limiting streamlines in Figure 24d, there is a clear increase in asymmetric flow separation. The area of flow going backwards seem to originate from the tubecles trough.

5.2 Foil A14W52.5

In the A14W52.5 study (Rostamzadeh et al., 2017) a NACA0021 foil is used. The NACA0021 has a maximum thickness of 21% of the chord length compared to 20% for the NACA0020 in section 5.1. There is also a difference at the leading edge which can be described as:

$$x_{LE} = 0.007 \cos\left(\frac{2\pi}{0.0525} z\right)$$

where 0.007 is half the amplitude of the tubercles, 0.0525 is the wave length and z is the position along the leading edge.

Rostamzadeh et al. (2017) used a flat leading egde to validated against where the results were experimental data. The validation foil Rostamzadeh used was also a NACA0021, but with the span width of 0.0105 m compared to the tubercle foil with a span width of 0.021 m. The method on which they validated the flat leading edge foil was to compare the pressure coefficient.

The tubercle foil Rostamzadeh et al. created is called A14W52.5 due to the amplitude of 14mm and wavelength of 52.5mm. Furthermore Rastamzadeh et al. have also provided data for drag and lift for a normal NACA0021 foil without tubercles.

In this section, a validation study for both the flat leading edge foil and the tubercle foil created by Rostamzadeh will be stated.

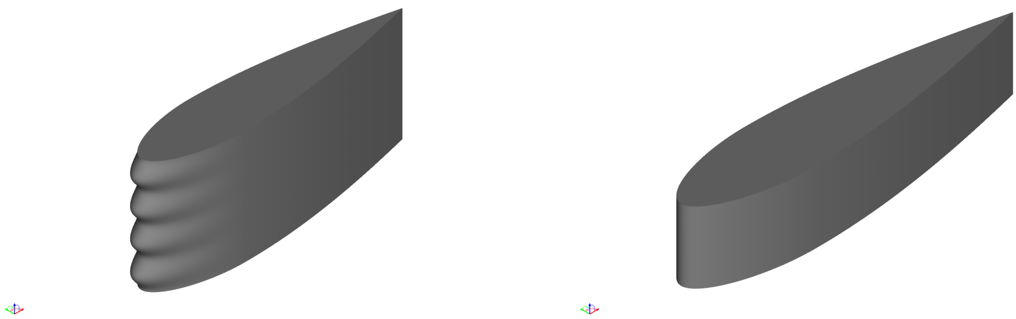

(a) Tubercles on leading-edge. **(b)** Flat leading edge.

Figure 25: Foils used in the A14W52.5 study.

The input data used for the A14W525 validation simulation can be seen in Table 8

Table 8: Main particulars for the A14W525 Validation Simulation.

Parameter	Abbreviation	Value
Chord Length	C	0.049 [m]
Span Width	S	0.021 [m]
Area	A	0.001029 [m^2]
Freestream Density	ρ	998 [$\frac{kg}{m^3}$]
Freestream Velocity	U	27.2 [$\frac{m}{s}$]
Dynamic Viscosity	μ	8.871E-4[$\frac{kg}{ms}$]
Reynolds number	Re	1,500,000
Desired y^+	y^+	1
Prism Layers	N	55
Prism Layer Thickness	L	0.005 [m]
Thickness of near wall Prism Layer	ΔS	7.91478E-7 m [m]

Lift- and drag plots

The CFD analysis results provided in the article is listed below in table 9, which are the results that the validation simulation will be validated against.

Table 9: CFD analysis results from (Rostamzadeh et al., 2017).

	A14W525		NACA0021	
AoA	C_L	C_D	C_L	C_D
2	0.194	0.008	0.198	0.009
4	0.353	-	0.355	-
6	0.573	0.011	0.597	0.010
10	0.994	0.016	0.951	0.016
14	1.356	0.029	1.274	0.025
18	0.884	0.182	1.409	0.052
20	0.934	0.210	1.354	0.079

The data from Table 9 (Rostamzadeh et al., 2017) was then combined with the present validation study simulation results in a plot illustrating C_L in Figure 26 and C_D in Figure 27.

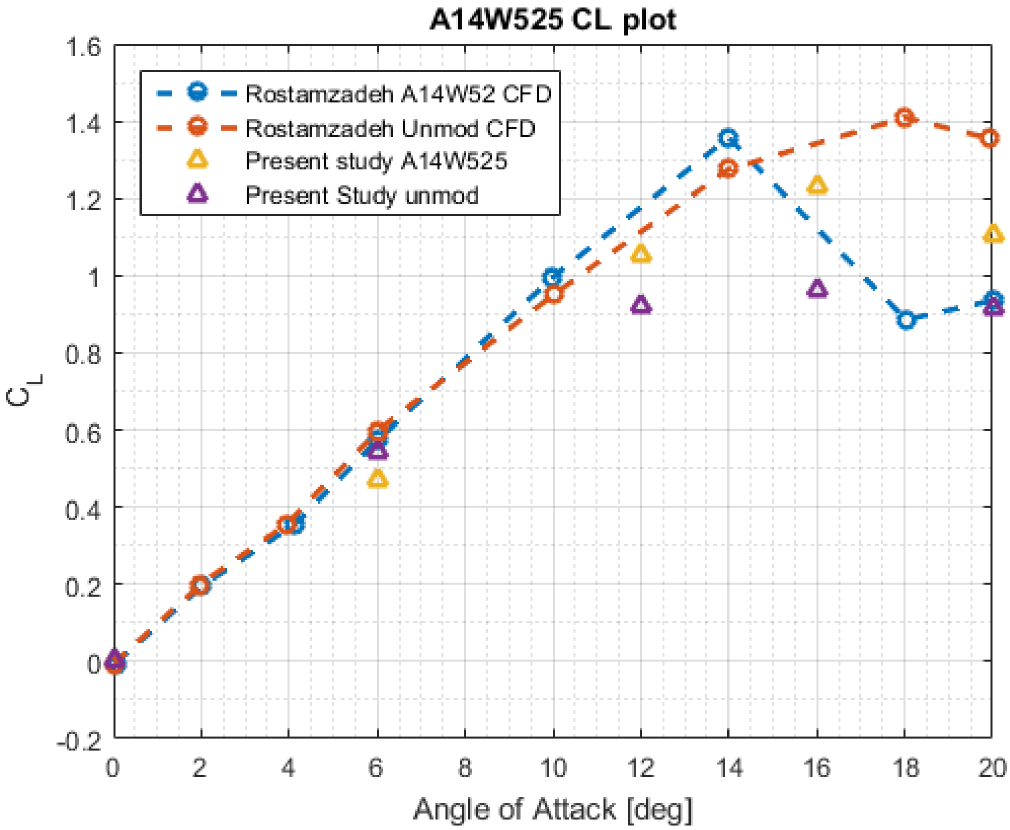

Figure 26: A14W525- and unmodified, straight leading edge, foil plotted together with present study A14W525 and unmodified, straight leading edge, foil.

It can be observed that there are differences at high AoA for the lift coefficient C_L in Figure 26. For Rostamzadehs CFD simulations of the A14W525 there is a sudden drop in C_L after 14° where the foil seems to stall. According to the current validation study, it starts decreasing its lift ability after 16°. However, it does not drop as low as Rostamzadehs CFD A14W52.5 foil. (Rostamzadeh et al., 2017).

Compared to the unmodified foil, the tubercle foil in Rostamzadehs case performs better for both C_L and C_D. C_D can be seen in fig 27 below. However, this is not the case in present study. The present study CFD results shows an improvement in lift compared to the unmodified leading edge simulation. C_D is equivalent to the unmodified foil until 12° where C_D increases above the unmodified foils C_D.

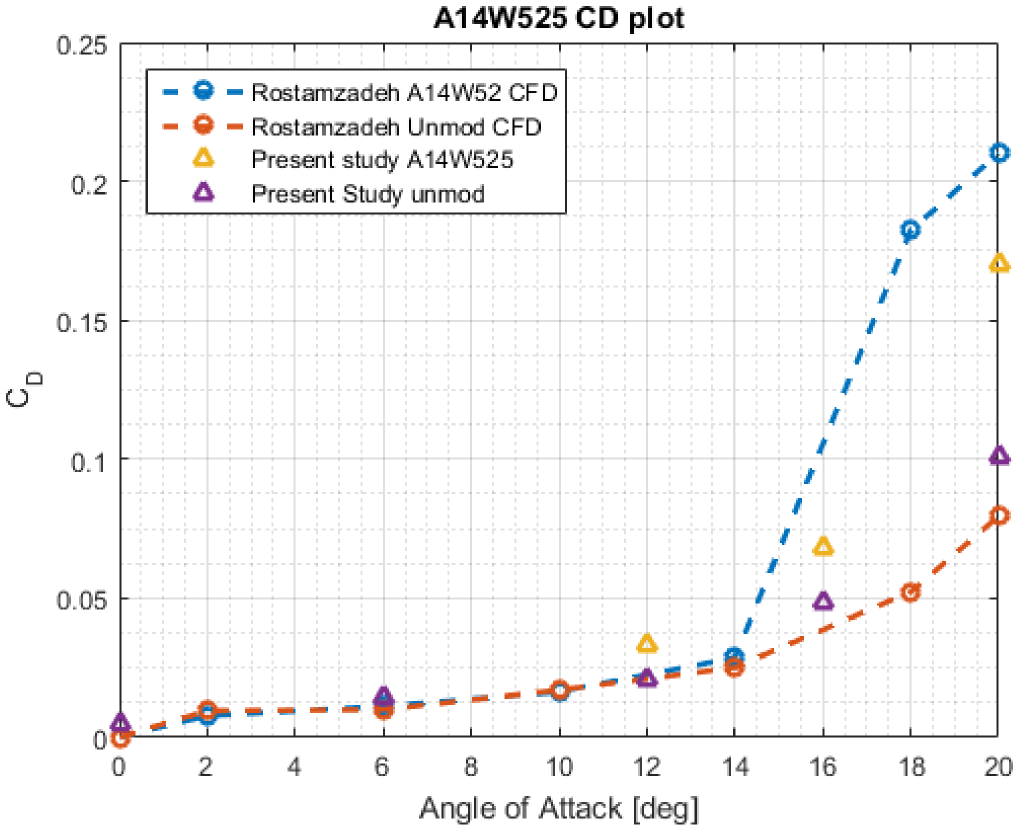

Figure 27: Rostamzadeh A14W52 and unmodified plotted together with present study A14W525 and unmodified.

Vorticity

In Figure 28, the iso-surface of vorticity along the foil is illustrated. The contours on these iso-surfaces show the velocity magnitude. As can be expected there is a lot of vortical strucures at high AoA compared to lower ones. As in the previous validation study, it took longer time for the results for converge compared to the lower AoA. The turbulent flow structures and the flow unsteadiness are reasons for longer convergence time in these comitations.

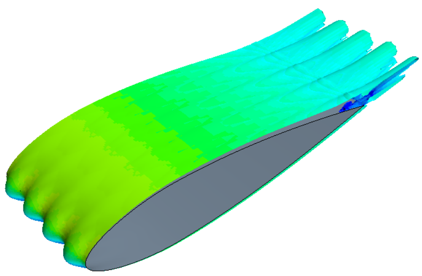

(a) AoA=6°.

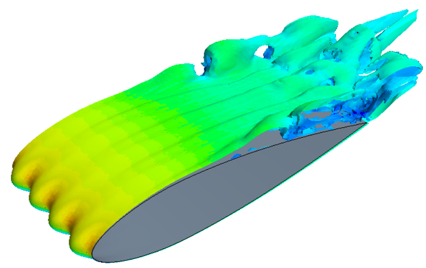

(b) AoA=12°.

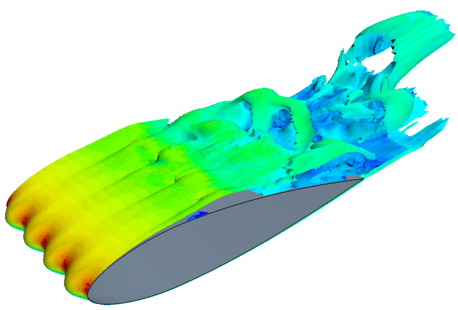

(c) AoA=16°.

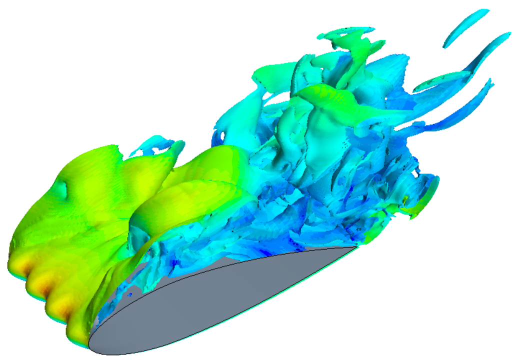

(d) AoA=20°.

Figure 28: Vorticity on the suction side of the foil.

At 6° the flow separation on the foil occur midway at approximately 0.9C. As the angle increases, more and more turbulence occur and flow separation occurs closer to the leading edge for every angle. This creates an area with large oscillating flow and lower pressure on the foil which influences the foil lift and drag.

Limiting streamlines

In this section, limiting streamlines are plotted to visualise the flow separation more clearly. The flat leading edge and A14W52.5 are plotted at AoA = 6° and 20°.

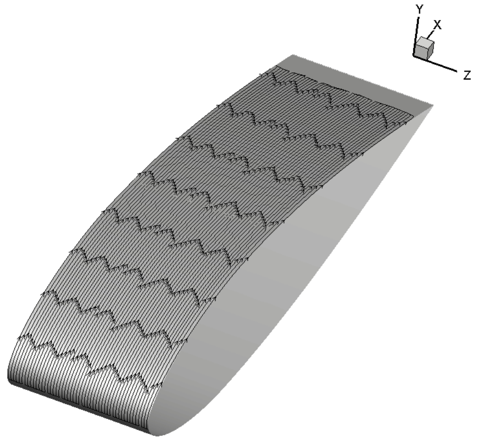

(a) AoA=6°.

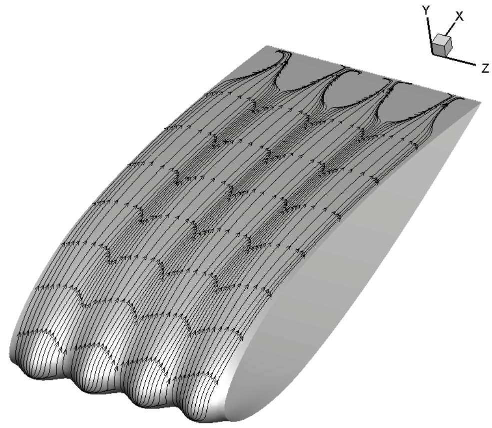

(b) AoA=6°.

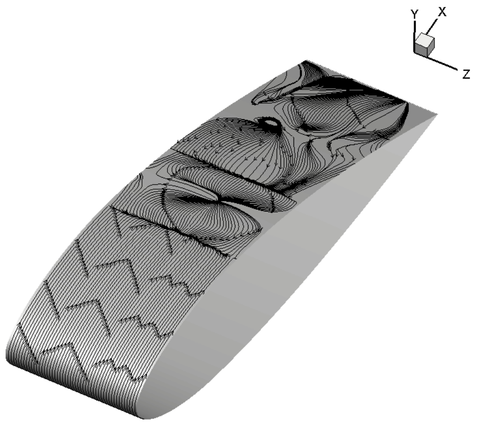

(c) AoA=20°.

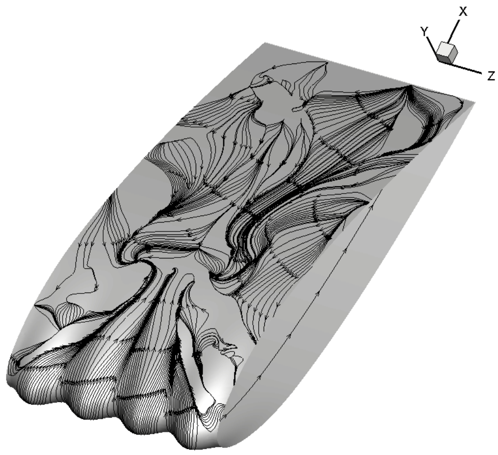

(d) AoA=20°.

Figure 29: Limiting streamlines for A14W52.5 and a flat leading edge foil.

The limiting streamlines in figure 29d show the same results as the vorticity in figure 28d. This helps confirm even further the large area of turbulent flow at high angles of attack. At AoA = 6° as seen in figure 29b and 29a there is only a small difference in flow pattern at the trailing edge. On the flat leading edge foil in Figure 29a, there is a small area of separation close to the trailing edge. However, interestingly A14W52.5 has attached flow until the trailing edge between the separation areas behind the tubercles. Comparing the foils at AoA = 20°in Figure 29c and 29d, the flat leading egde show a flow sepration roughly halfway down the chord length. However, for the tubercled foil, the limiting streamlines show a massive area of flow separation. This indicated a higher drag coefficient compared to the flat leading egde.

Pressure Coefficient plot

In the Rostamzadeh study of the pressure coefficient along the suction and pressure side for a straight leading edge NACA0021 foil is given for 6°, 12°, 16° and 20°. Moreover, they compared their computed C_p data from Gregorek (Hoffman and Berchak, 1989). The values from the present study are plotted next to the values from the A14W52.5 study as well as the Gregorek experimental data in Figure 30 to 33. The pressure is shown along the chord length of the foil.

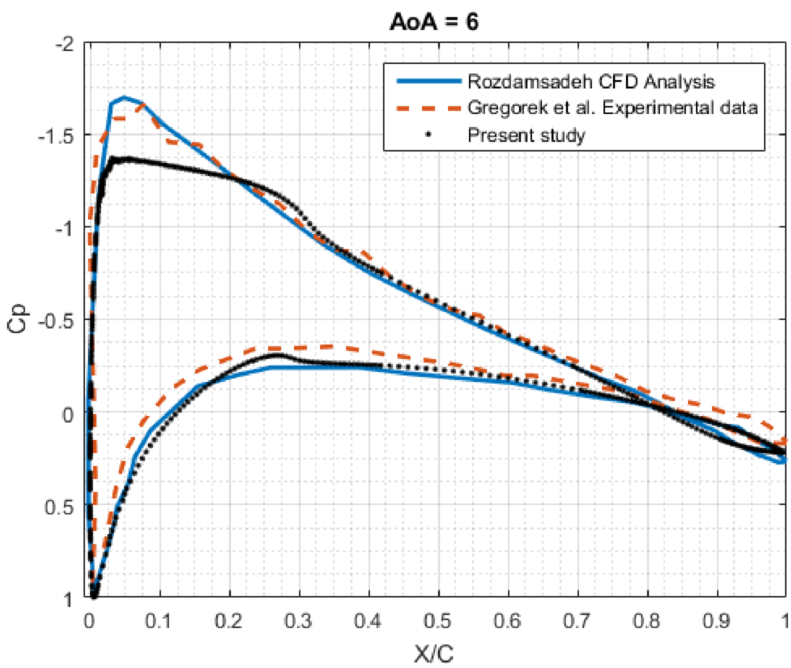

Figure 30: Gregorek experimental data, Rostamzadeh and present study plotted together for 6° (Hoffman and Berchak, 1989), (Rostamzadeh et al., 2017).

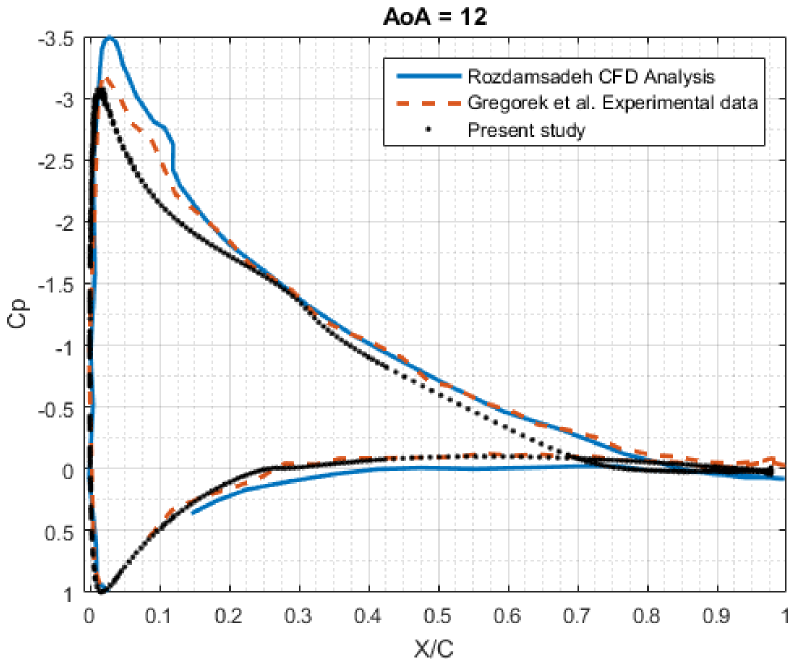

Figure 31: Gregorek experimental data, Rostamzadeh and present study plotted together for 12°(Hoffman and Berchak, 1989), (Rostamzadeh et al., 2017).

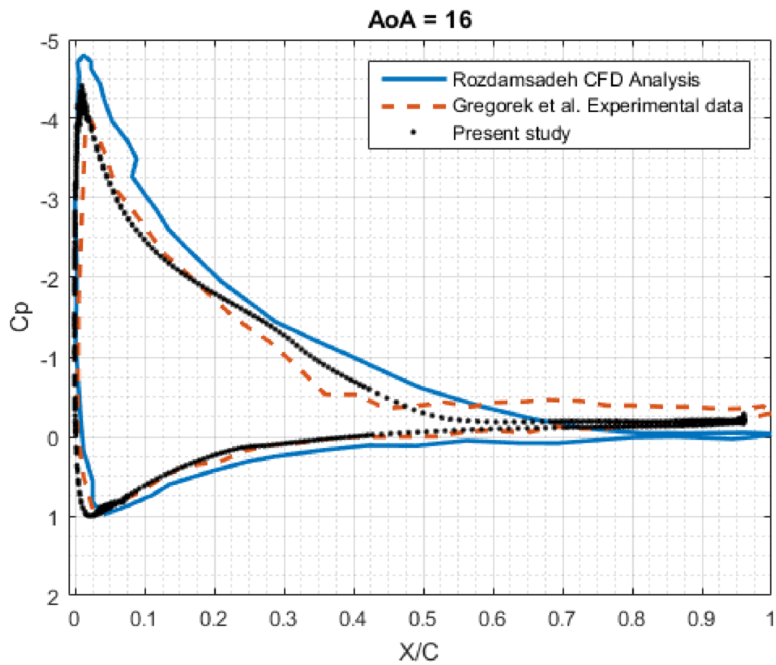

Figure 32: Gregorek experimental data, Rostamzadeh and present study plotted together for 16°(Hoffman and Berchak, 1989), (Rostamzadeh et al., 2017).

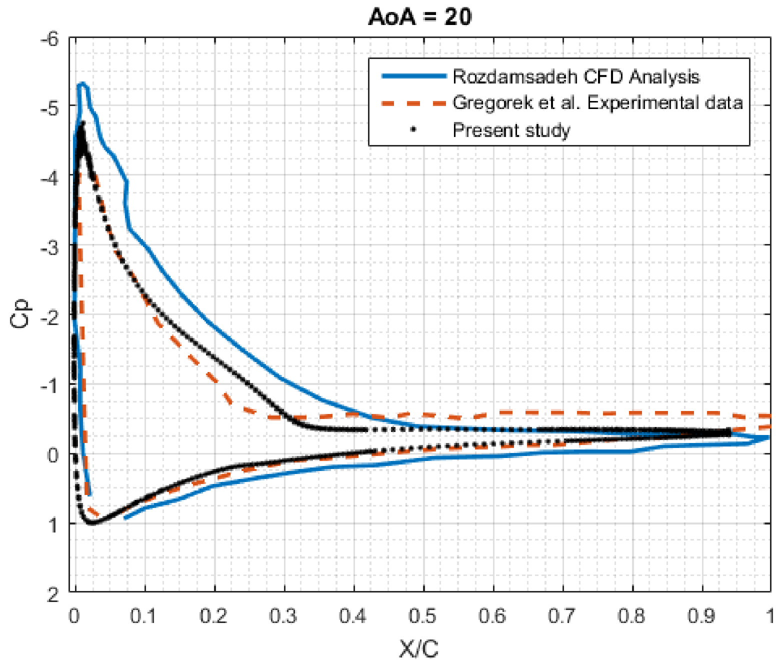

Figure 33: Gregorek experimental data, Rostamzadeh and present study plotted together for 20°(Hoffman and Berchak, 1989), (Rostamzadeh et al., 2017).

The seemingly shorter chord length in figure 31, 32 and 33, is due the angle of the foil and the cordinate system used. The foil itself has the same C as Rostamzadeh and Gregorek et al foils, but relative to X-axis in present study makes it appear to have different C altought they are equal.

At all cases, the present study CFD simulations are closer to the experimental data on the pressure side of the foil. Rostamzadeh have managed closer results to the experimental data on 12° as seen in figure 31 (Hoffman and Berchak, 1989).

It is worth noticing that Rostamzadehs CFD is conducted using SST k-ω turbulence model while present authors used Spalart-Allmaras. We also studied the effect of the SST K-omega turbulence model on the results at 6°and 20°AoA in the comparison to the Spalart-Allmaras turbulence model. Negligible differences between C_p were observed at 6°which was not the case for 20°of AoA. The pressure coefficient obtained from these turbulence models deviated from each other in the vicinity of the stagnation point. Our CFD predictions show 7% lower C_P over all, than Rostamzadeh's CFD simulation, but therefore closer to the experimental data given by Gregorek. This is also a reason for using Spalart-Allmaras in current CFD and not SST k-ω as Rostamzadeh did.

5.3 Foil Weber et al.

In (Weber, Laurens, et al., 2011) a case study was done on a foil very similar to a real humbpack whale flipper. The base is a NACA0020 which is a foil that resembles a real flipper the most. To describe the leading-edge, equation 8 and trailing-edge equation 9 were used.

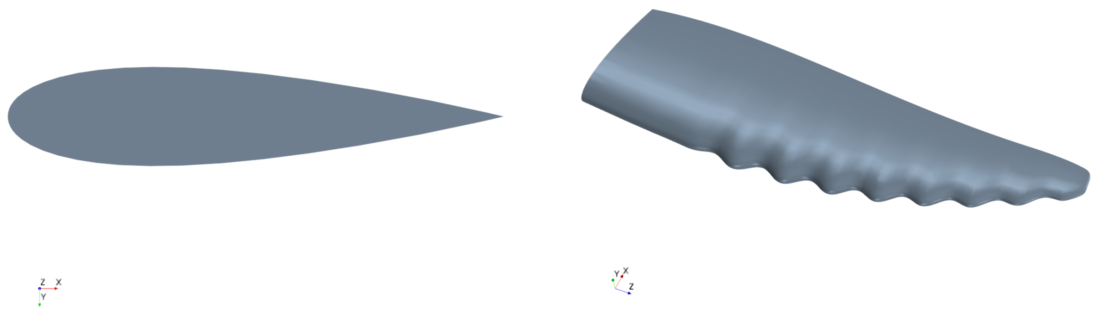

(a) NACA0020 baseline foil shape. **(b)** 3D Geometry scene.

Figure 34: Flipper used for Weber et al. simulations.

$$X_{LE} = 2.916 + 0.0624y + 0.000428y^2 + 0.000462y^3 \tag{8}$$

$$X_{TE} = \begin{cases} -3.152 - 0.113y + 0.0194y^2 - 0.000552y^3, & \text{y <19.98 in} \\ -0.375\sqrt{1 - 0.158(y - 19.98)^2} - 1.7, & \text{y} \geq \text{ 19.98 in} \end{cases} \tag{9}$$

The input data used for the Weber validation study can be seen below in Table 10

Table 10: Main particulars for Weber Validation Simulation.

Parameter	Abbreviations	Value
Chord Length	C	0.01305 [m]
Span Width	S	0.5607 [m]
Area	A	0.073765 [m^2]
Freestream Density	ρ	1.103 [$\frac{kg}{m^3}$]
Freestream Velocity	U	66 [$\frac{m}{s}$]
Dynamic Viscosity	μ	1.85508E-5 [$\frac{kg}{ms}$]
Reynolds number	Re	500,000
Desired y^+	y^+	1
Prism Layers	N	55
Prism Layer Thickness	L	0.005 [m]
Thickness of near wall Prism Layer	ΔS	5.719E-6 m [m]

The tubercles were modelled by an equation given in the article Howle et al. (Weber, Howle, et al., 2010)and can be seen in equation 10.

$$\begin{aligned} &\frac{X_{LE}}{S} = -\frac{1}{2^3}\left(\frac{3^2}{5} - \frac{A}{2^2}cos\left[2\pi\left(n+\frac{1}{2}\right)\frac{z}{S}+\chi\right]\right) \\ &\forall \quad 0 \leq \frac{z}{S} \leq 1 \end{aligned} \tag{10}$$

The domain recreated was a wind tunnel with a cross-section of 137x97cm with a length of 239cm. This was recreated in present study validating simulations (Weber, Laurens, et al., 2011). The article states that incompressible flow was assumed and a Re = 505 000 to 550 000 were used. The wall boundary condition was used for every boundary.

Figure 35 show the computational domain as well as the mesh which has the same dimension as the experiment and CFD simulations as stated in Weber et al. (Weber, Laurens, et al., 2011). Mesh size is 2.9 million cells.

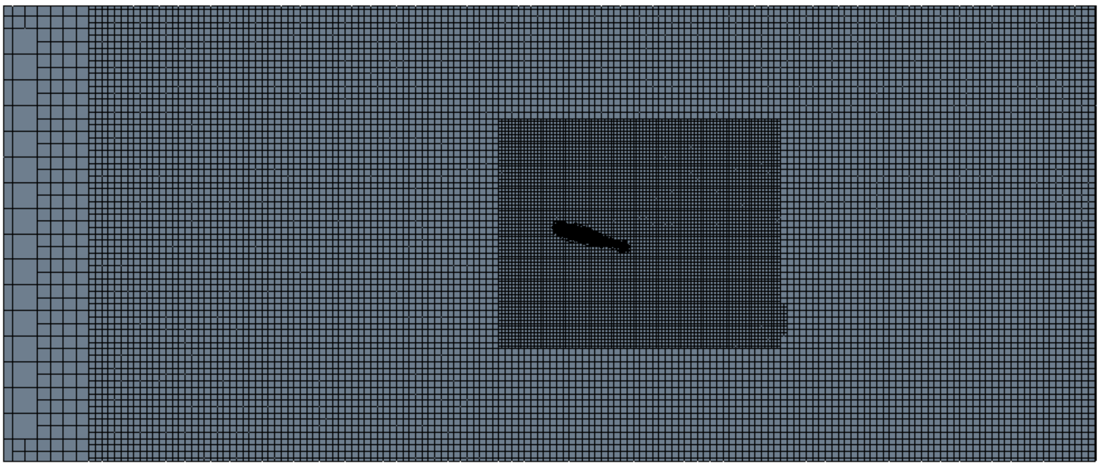

Figure 35: Computational domain with mesh.

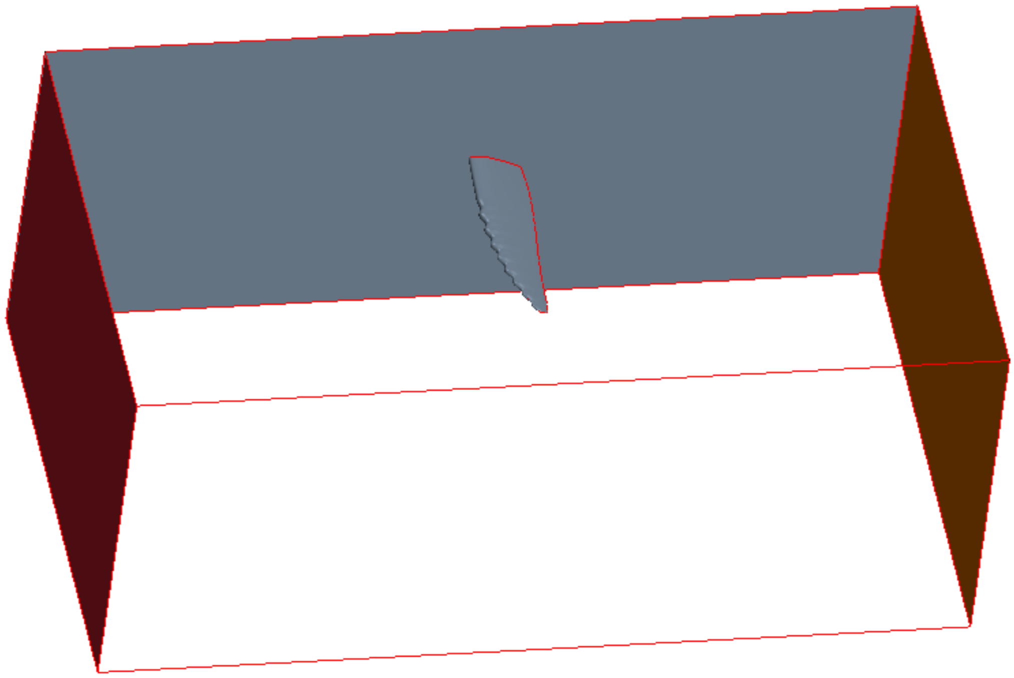

Figure 36: Computational domain as the Wind tunnel from Howle et al. (Weber, Laurens, et al., 2011).

After replicating the exact conditions in present study, the result where simulated as shown in figure 37 and 38.

The values of C_L in Figure 37 is similar for angles below 10°. For angles higher than 10° there is a noticeable difference between the Webers CFD results and the present study results. There is also a difference from Webers and their own experimental data. At 16°, the experimental data is higher than both current CFD and Webers CFD. But, at 18° and 20° current CFD results are closer to the experimental data from their wind tunnel tests.

When evaluating C_D in Figure 38, the difference between Webers CFD and current CFD results are small. It shows again that the high oscillation levels found at high AoA increase the computational difficulty.

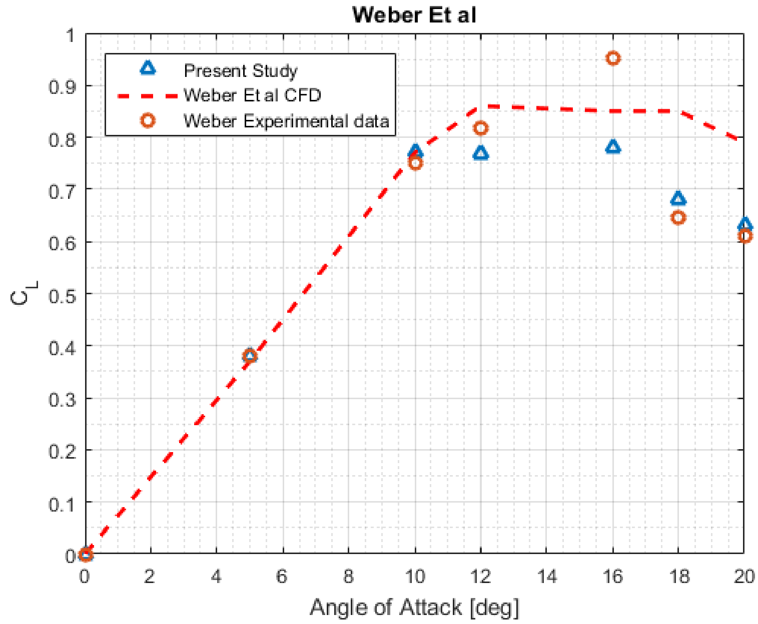

Figure 37: Results for C_L from the Validation foil simulation.

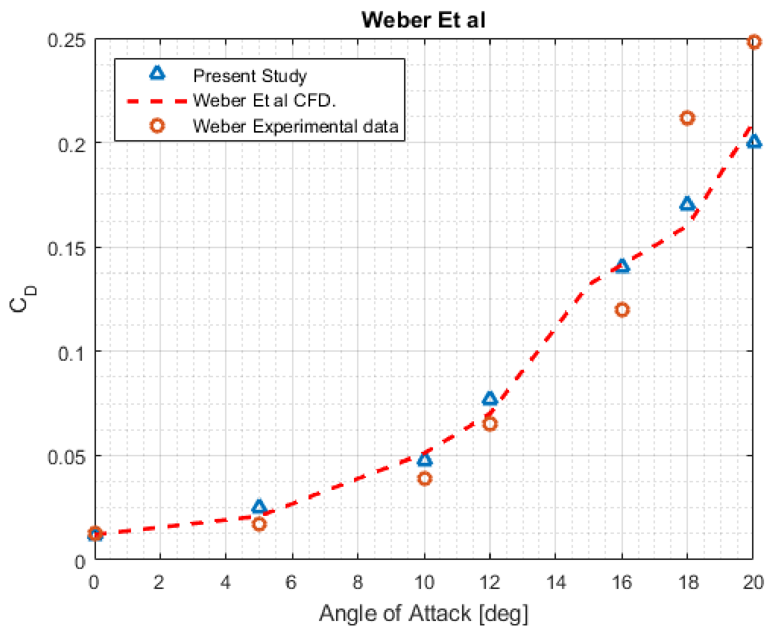

Figure 38: Results for C_D from the Validation foil simulation.

A source for the difference may be that in present study the cell count is 2.9 million cells while Weber, Laurens, et al. (2011) used at most 2.3 million cells in order to decrease the computational time. When Weber et al. changed the cell count from 1.4 million cells to 2.3 million, they observed a difference in 10% for C_L and 3.2% for C_D. However, to get a mesh that represented the shape accurate in STAR-CCM+, at least 2.9 million cells had to be used.

5.4 Conclusion of Validation study

In the previous section all the data from the present study simulations from STAR-CCM+ has been presented and compared with all three articles which was chosen to validate against. In this section a short recap of the result of the validation studies will be presented.

When observing all three cases; 4878 (Lohry et al., 2012), A14W52.5 (Rostamzadeh et al., 2017) and Weber et al (Fish, Weber, et al., 2011) there is a common factor observable in Figure 20, 27, and 38. This is how well the calculation, from STAR-CCM+, of the drag coefficient aligns with the drag coefficient data provided in all three cases.

Case A14W52.4 in Section 5.2 is particularly interesting as the authors of the articles have not validated against previous tubercle foil simulations, but rather physical experimental data of a standard flat leading edge foil. They are plotted in Figure 30 to 33 and represent the pressure coefficient over the suction and pressure side of the foil. Here the peak values generated by present authors are closer to the experimental data than Rostamzadeh and their CFD simulations are. They have in the 12° case shown in Figure 31, a more accurate calculation of the suction side. However, all other AoA, the present study CFD have shown to be closer to the experimental data provided by Hoffman and Berchak (1989). The lift coefficient has been more difficult to validate. As mentioned, the high level of turbulence and thus oscillating flow has caused some difference in post-stall regions, i.e 12° and higher. This can be seen in Figure 19, 26 and 37 which show the results for the lift coefficient from all three cases. It is observable at low angels of attack that both present CFD simulations in STAR-CCM+ and the CFD results from case A14W52.5 in Section 5.2 and case 4878 in Section 5.1 coincide well up to 16° before the graphs diverge from each other.

In figure 28 the oscillations are modelled by STAR-CCM+ in 3D to get a clearer understanding of exactly what is happening when the fluid separates from the foil. It also helps in understanding why the difference in C_D at high AoA occur. In figure 28d one can see the separation at 20° where the flow separates almost immediately at 0.1C.

In all validation cases the turbulence model described by the validation article were also used in all simulations done by present study except for case A14W52.5. Using the turbulence model SST k-ω from Section 3.5.1.2, the result showed poor resemblance to the validation studies and this is why the Spalart-Allmaras model was chosen instead. This gave, as seen in the result plots, better accuracy towards the experimental data provided by Gregorek.

After reviewing the results from all three validation cases, the authors of this thesis believe that the set up in STAR-CCM+ is valid, and approved to move on to an optimisation of a foil with leading edge tubercle design.

6 Results

In this chapter the results from the simulation of lift- and drag coefficient for the foils designed will be presented. The main particulars for the domain and foils can be found in Table 2 in Section 4.2.3. The lift-, drag. and lift-to-drag ratio plots will be illustrated for all of the investigated foils while further results will be presented for the top two foils as well as a flat- and the worst performing foil. Furthermore the pressure coefficient, vorticity field, velocity profile and limiting streamlines will be presented for a selection of foils.

Please note that there is no result for the foils with 4 tubercles. This is due to an error in the coupling of CAESES© and STAR-CCM+. The error destroyed the tessellation on the foil making it impossible to create a surface mesh. Therefore these foils have been excluded from the results.

6.1 Lift-to-Drag ratio

Figure 39 shows the lift coefficient, C_L, for the foils investigated.

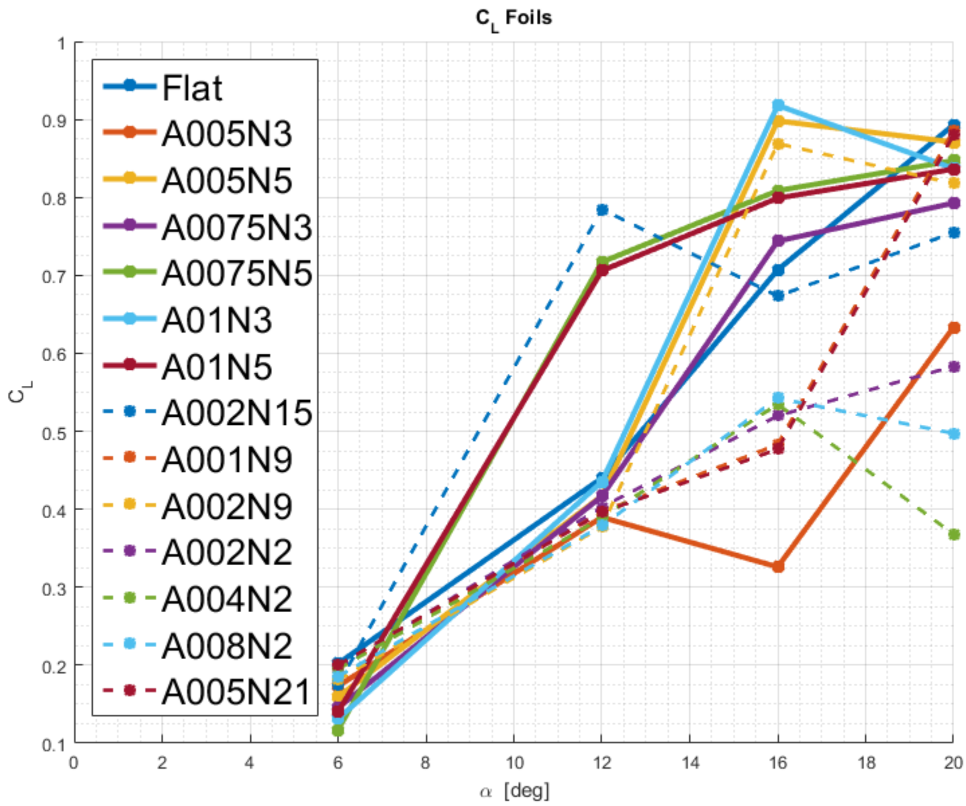

Figure 39: C_L for different foils and different AoA.

Figure 40 shows the drag coefficient, C_D, for the foils investigated.

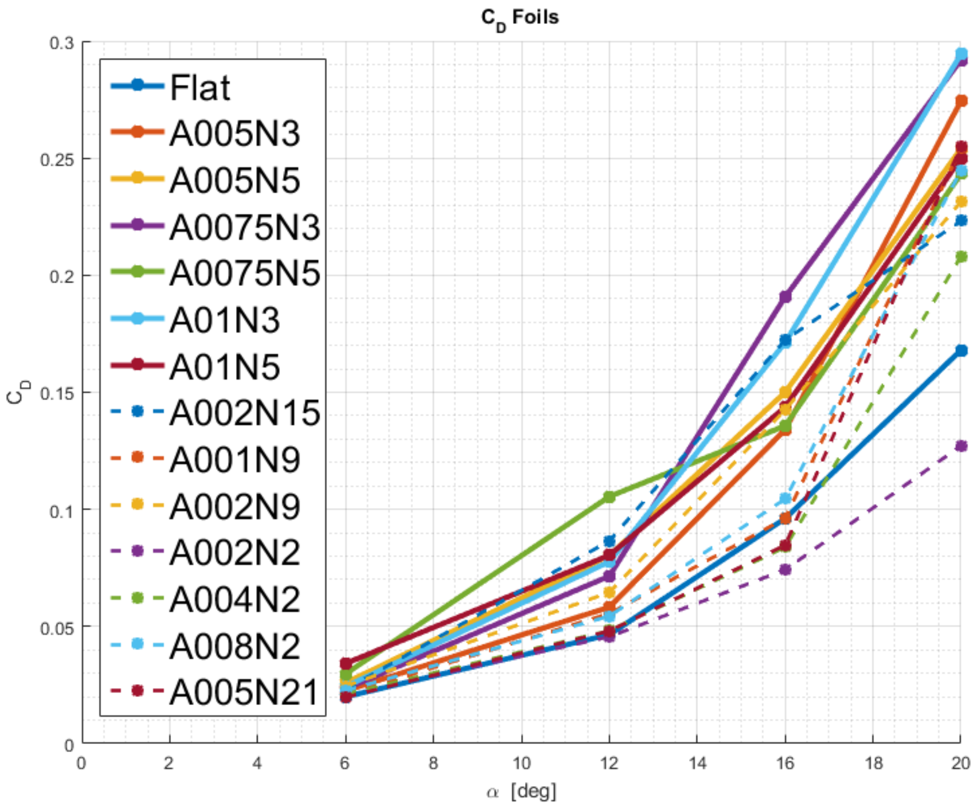

Figure 40: C_D for different foils and different AoA.

In Figure 41 are the lift-to-drag ratio presented for all the foils that were examined. None of the three foils that produce most lift are in the top of the lift-to-drag ratio. Further it is interesting to see that the foil with the flat leading edge is the one with the highest lift-to-drag ratio over the entire span of AoA.

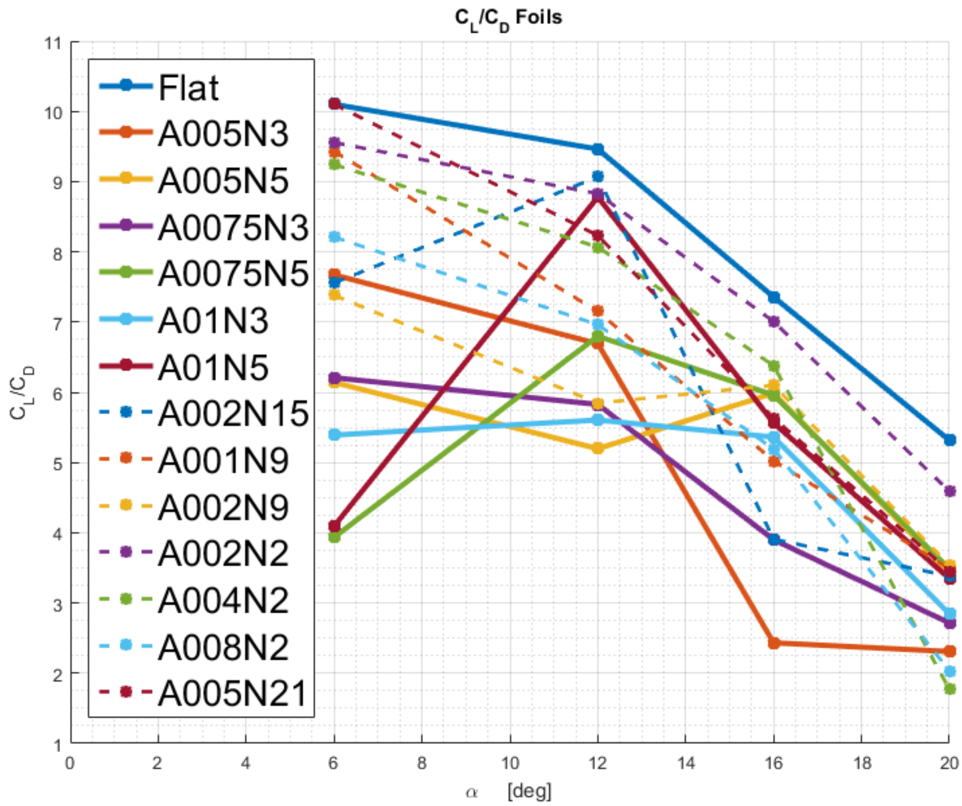

Figure 41: Lift-to-Drag ratio for different foils and different AoA.

To simplify, further comparisons will only be made with three different foils with tubercles on the leading edge. Two of these foils will be high performing and the third will be the foil with the lowest performance in regards to the lift-to-drag ratio. The foils will be compared to the flat leading edge foil. The two foils performing best are A002N2 and A005N21 and the worst performing is A01N3.

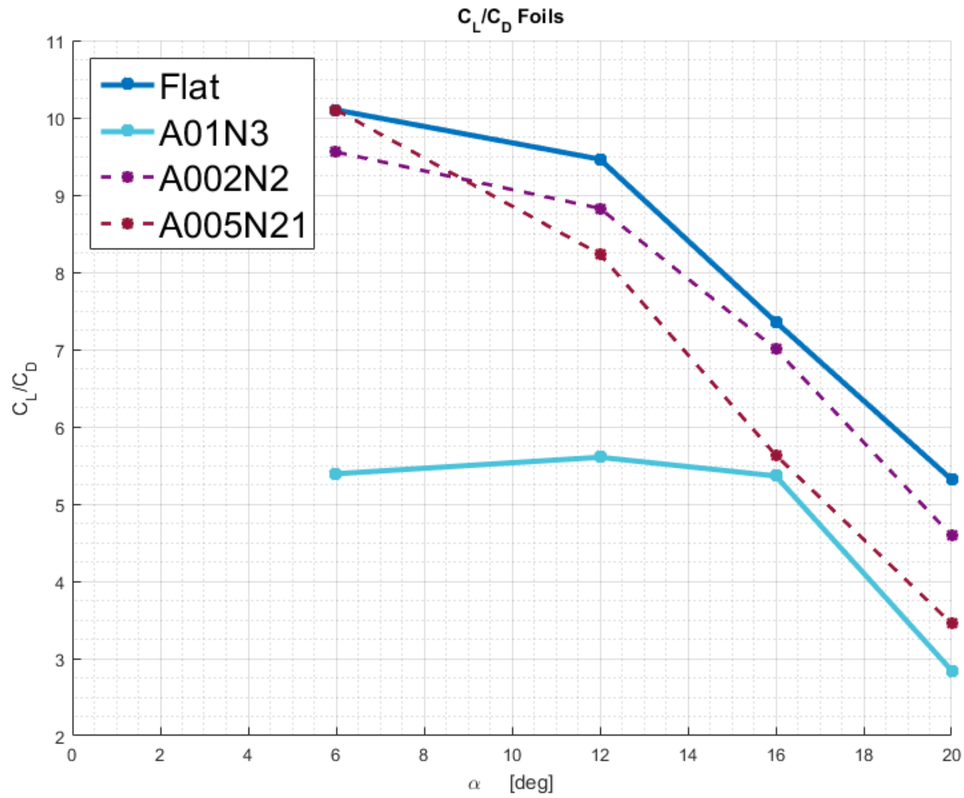

Figure 42: Lift-to-drag ratio plot for a flat foil, the two best and the worst foil.

6.2 Vorticity Field & Limiting Streamlines

In this section the vorticity in the spanwise direction and velocity of these vortices is presented as well as the limiting streamlines. The separation of the flow is visible on the suction side of the foil and the difference in separation between different foils and AoA. Next to the figure of the vorticity the corresponding limiting streamline is presented. The limiting streamline can be seen as a compliment for understanding the separation of the flow. The figures can then be compared with the plots of the pressure coefficient C_p, in Section 6.3, where the position of separation is seen as the drastic drop of C_p. The foils will be presented from best to worst performance: Flat leading edge, A002N2, A005N21 and finally A01N3.

6.2.1 Foil with Flat leading edge

In Figure 43 the vorticity and the velocity of the vorticity is presented for the foil with flat leading edge. The separation can be seen clearly as the region where the velocity drops and the isosurface separates from the flow. Looking at the limiting streamlines it is even clearer where the separation occurs. The separation occurs more or less at the same chord length position along the entire spanwidth, as mentioned in chapter 2 and 5.

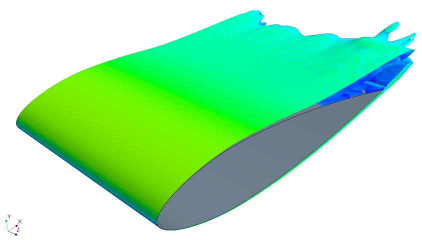

(a) AoA = 6°.

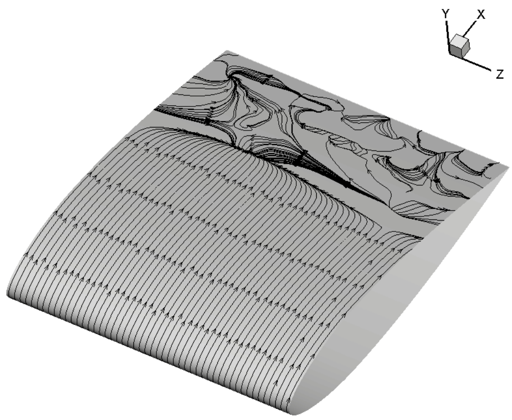

(b) AoA = 6°.

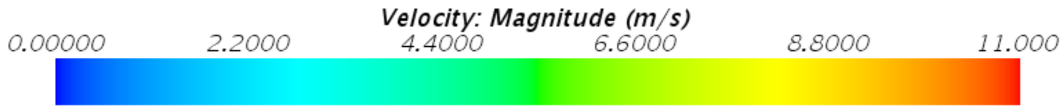

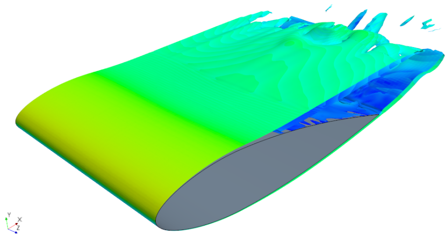

(c) AoA = 12°.

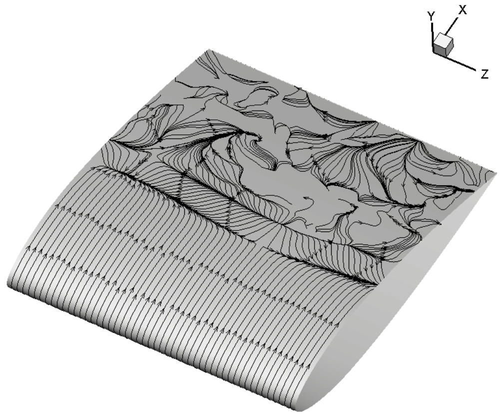

(d) AoA = 12°.

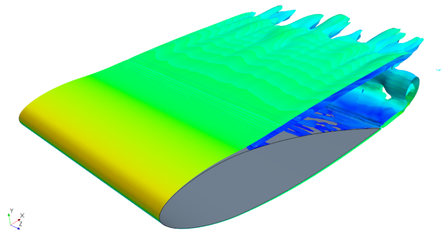

(e) AoA = 16°.

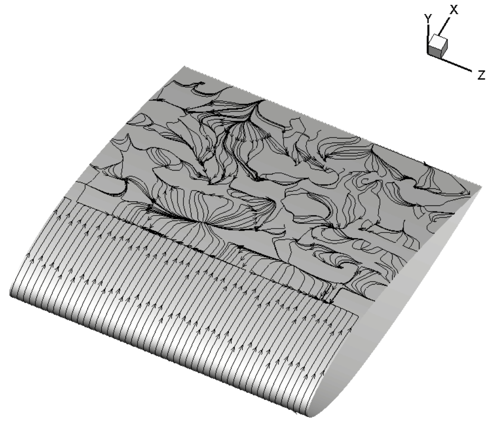

(f) AoA = 16°.

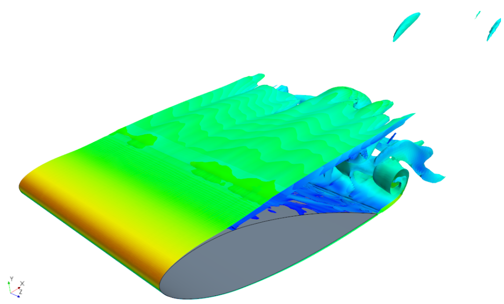

(g) AoA = 20°.

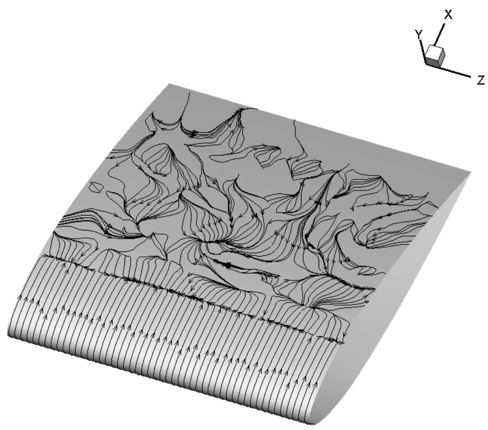

(h) AoA = 20°.

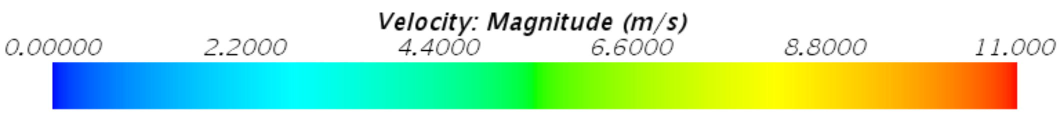

Figure 43: Vorticity and Limiting Streamline for foil with flat leading edge.

Foil A002N2

According to the lift-to-drag ratio plot in Figure 42 is A002N2 the foil with tubercles that show the most promising results. The tubercles for this foil have a small amplitude as well as a long wavelength, making it similar to a flat foil. For the low angles in Figure 44a and 44c the iso-surface of vorticity is similar to that of the flat leading edge at the same AoA. However, at higher AoA in Figure 44e and 44g the extent of iso-surface vorticity is larger for the foil with tubercles in comparison to to the foil with flat leading edge at the same AoA. This indicates the existence of a larger separation bubble for the foil with tubercles. Compared to the foil with the flat leading edge the flow does not separating at the same chord length position along the entire span width.

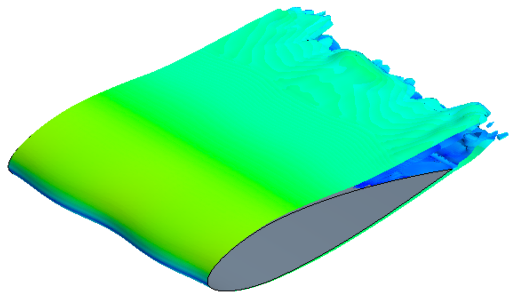

(a) AoA = 6°.

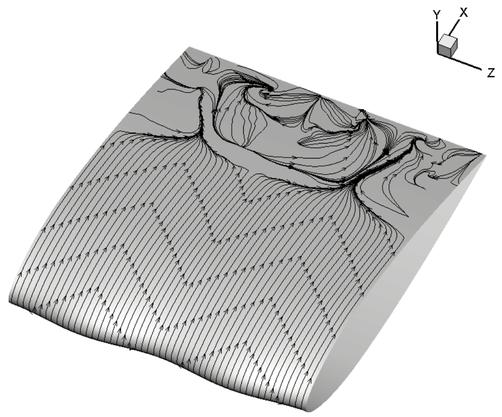

(b) AoA = 6°.

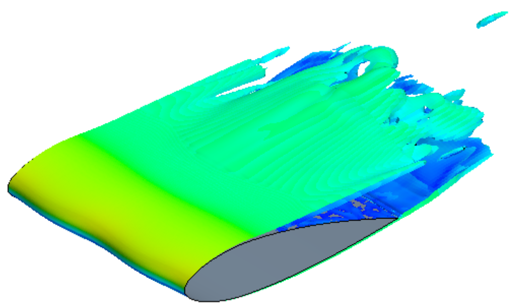

(c) AoA = 12°.

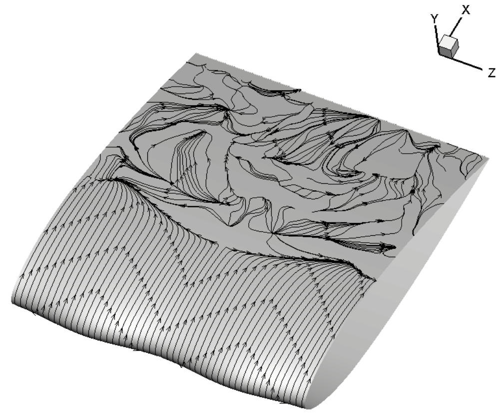

(d) AoA = 12°.

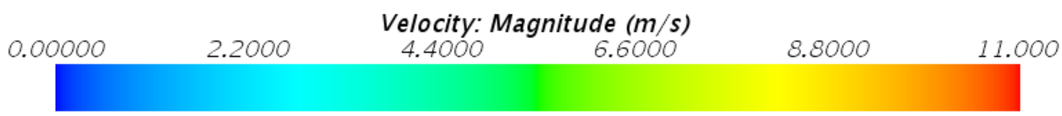

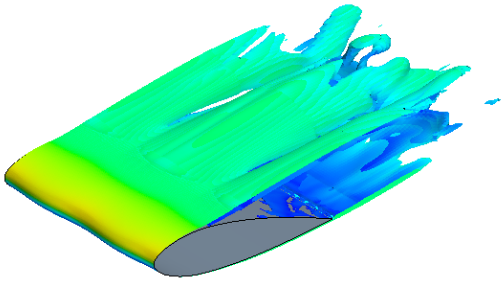

(e) AoA = 16°.

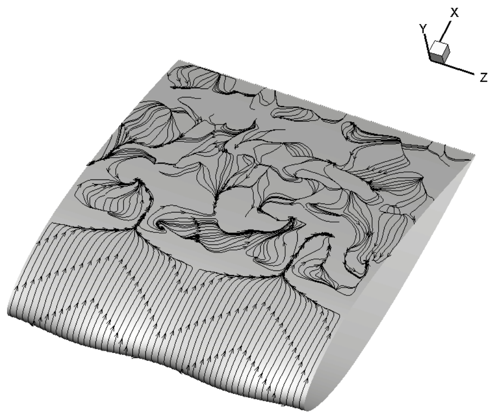

(f) AoA = 16°.

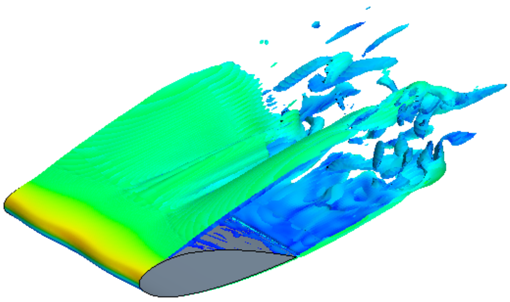

(g) AoA = 20°.

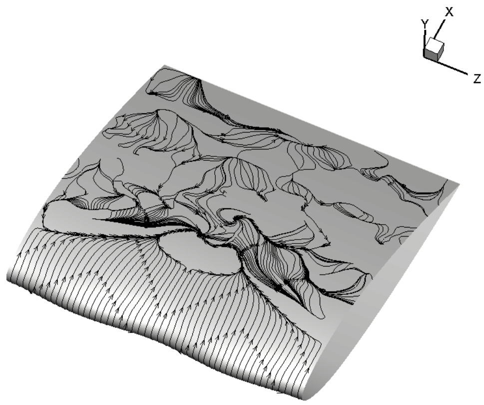

(h) AoA = 20°.

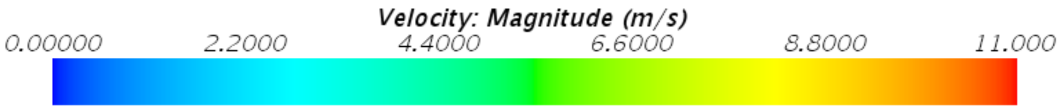

Figure 44: Vorticity and Limiting Streamline for foil A002N2.

Foil A005N21

A005N21 is the second best performing foil with tubercles. Like A002N2 the tubercles have a low amplitude but in this case is the wavelength short. This results in a foil that still resemble the flat leading edge foil a lot. This design results in quite smooth flow at 6°, 12° and 16°. However, at 20° the flow becomes very turbulent, see Figure 45g. This means that the separation bubbel is larger and more coherent than for the low AoA. At the same time does the drag coefficient increases severely as can be seen in Figure 40.

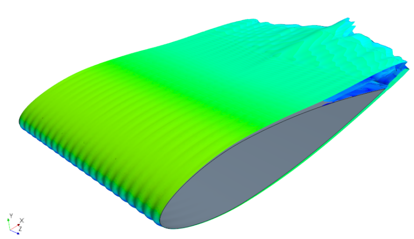

(a) AoA = 6°.

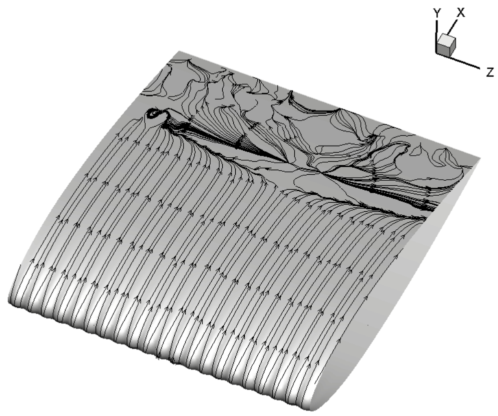

(b) AoA = 6°.

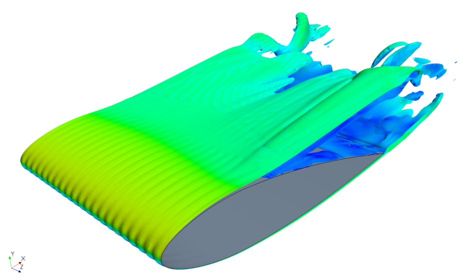

(c) AoA = 12°.

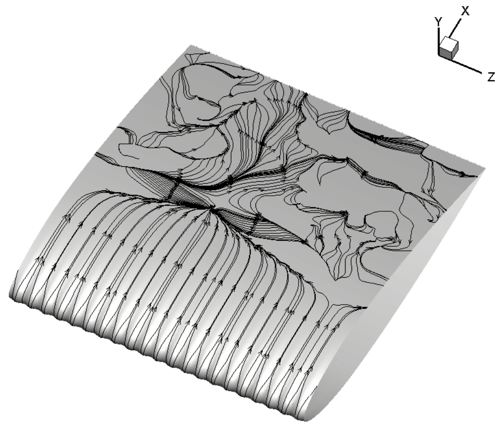

(d) AoA = 12°.

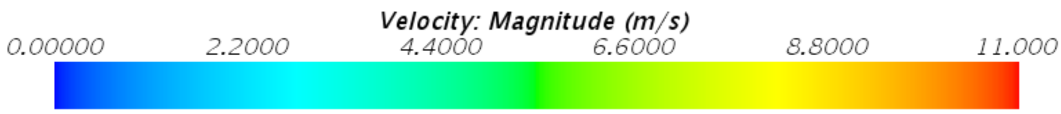

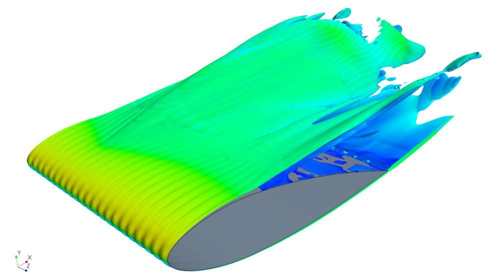

(e) AoA = 16°.

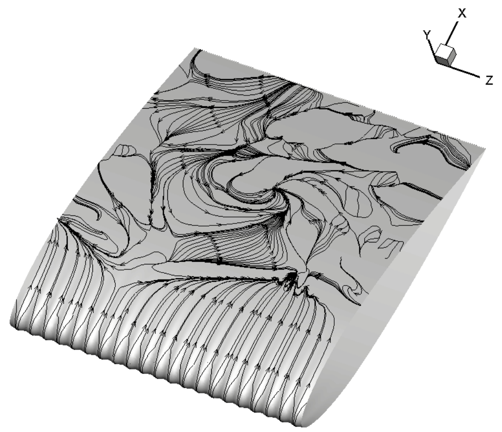

(f) AoA = 16°.

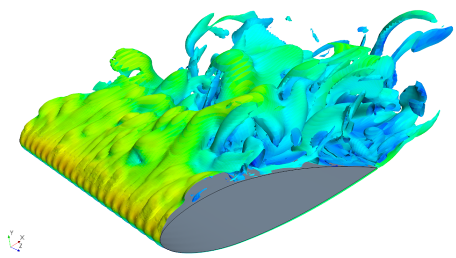

(g) AoA = 20°.

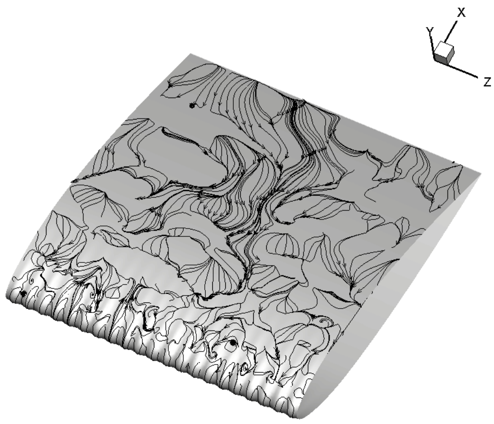

(h) AoA = 20°.

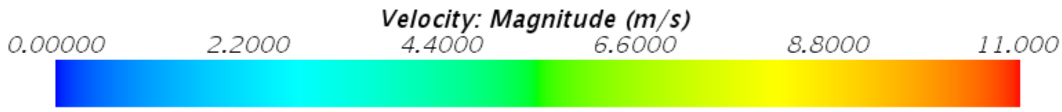

Figure 45: Vorticity and Limiting Streamline for foil A005N21.

Foil A01N3

Foil A01N3 is the foil with the worst performance. By looking at Figures 46 where the separation for different AoA is presented it is clear that there are more turbulence for this design. Already in Figure 46c for 12° there are a lot of separation and turbulence. Looking again at the drag coefficient in Figure 40 there is a rapid increase of the drag starting at 12° which correspond well to the figures of the vorticity iso-surface.

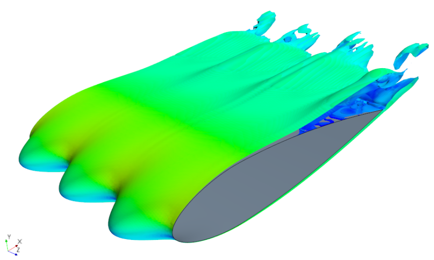

(a) AoA = 6°.

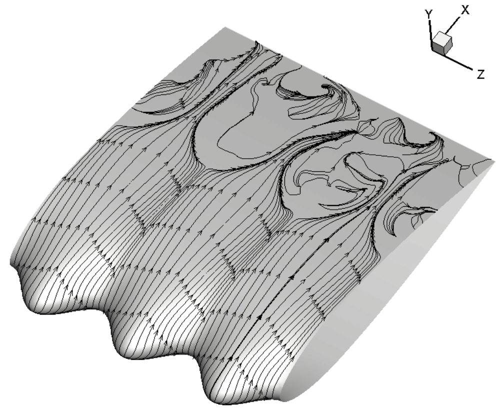

(b) AoA = 6°.

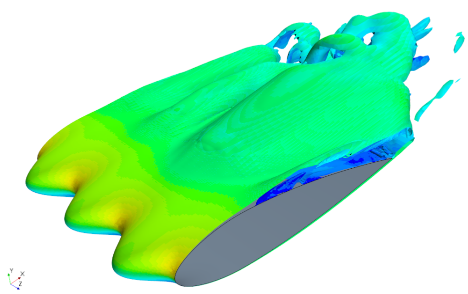

(c) AoA = 12°.

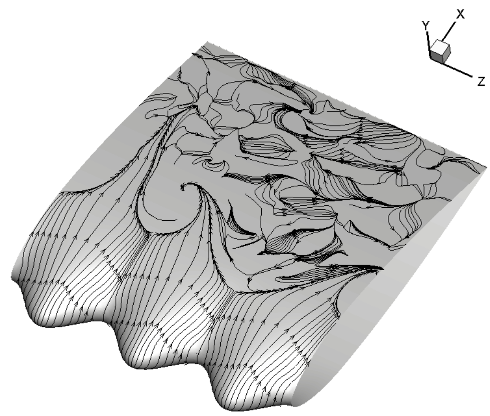

(d) AoA = 12°.

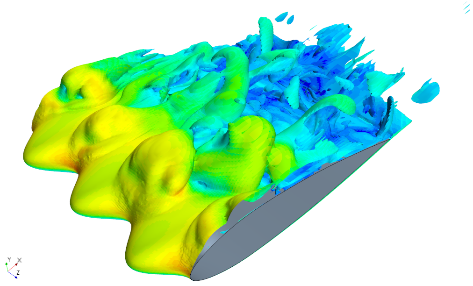

(e) AoA = 16°.

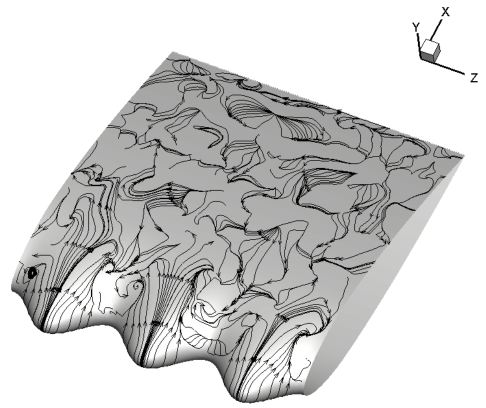

(f) AoA = 16°.

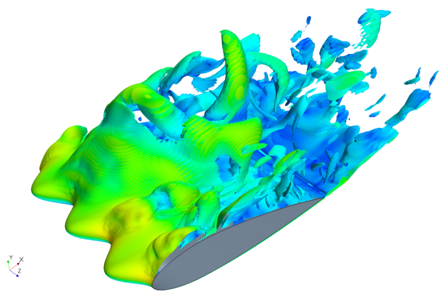

(g) AoA = 20°.

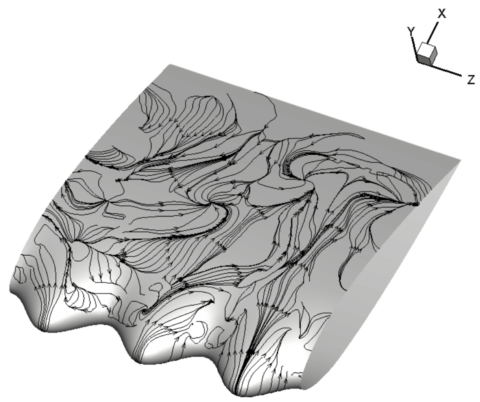

(h) AoA = 20°.

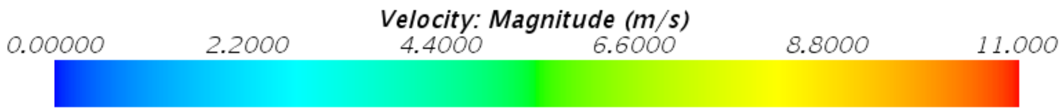

Figure 46: Vorticity and Limiting Streamline for foil A01N3.

6.3 Pressure Coefficient

In this subsection the pressure coefficient, C_P will be plotted for all 4 foils. For foil A002N2, A005N21 and A01N3, both tubercle peak and trough will be plotted, which also are the reason why different lines begin in front and some begin behind. This depends on the foil and the tubercle amplitude.

The pressure coefficient plots helps to understand the vorticity and the limiting streamline plots in the previous section. The pressure coefficient is plotted with negative values upwards on the Y-axis. The almost flat pressure coefficient (close to zero) on the suction side of the foil shows the extentof the separation region.

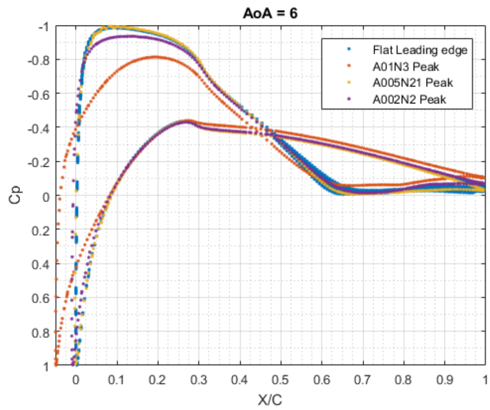

(a) Peak AoA = 6°.

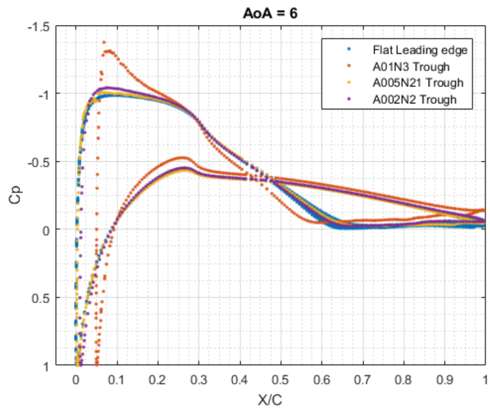

(b) Trough AoA = 6°.

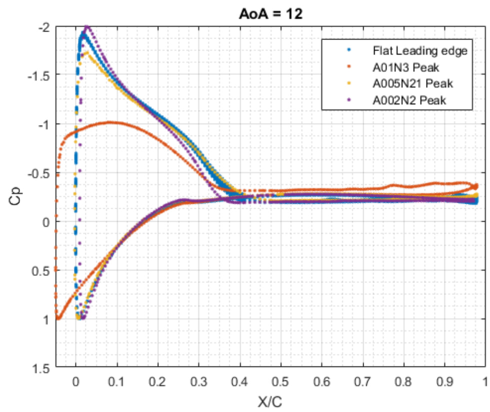

(c) Peak AoA = 12°.

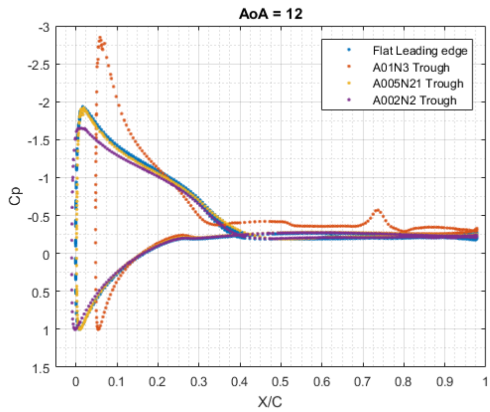

(d) Trough AoA = 12°.

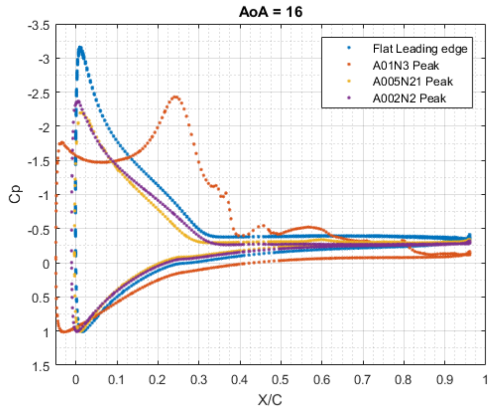

(e) Peak AoA = 16°.

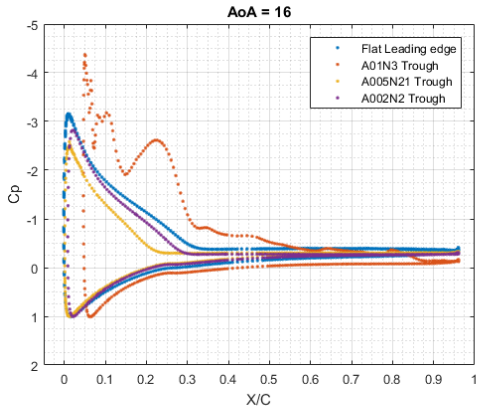

(f) Trough AoA = 16°.

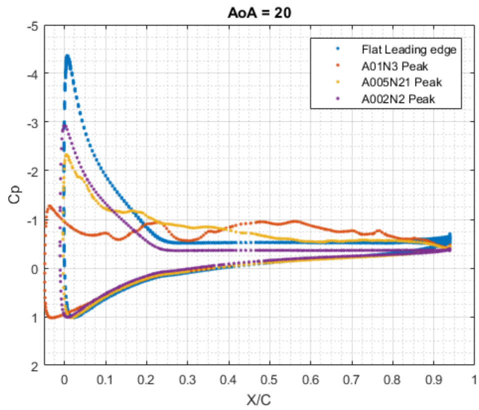

(g) Peak AoA = 20°.

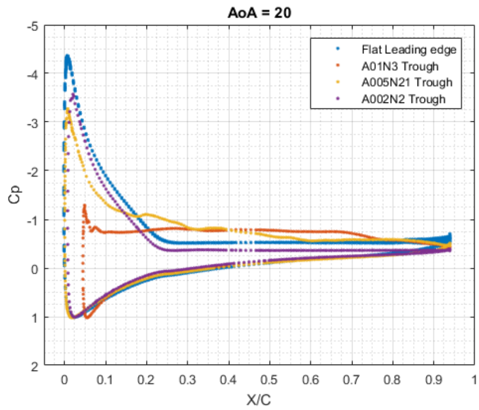

(h) Trough AoA = 16°.

Figure 47: Pressure coefficient for investigated foils at peak and trough.

The regular trend, which Weber and Howle reported, is that the pressure over the flat leading edge is between the values for peak and trough of a tubercle leading edge. However, at high AoA the pressure on the flat leading edge is lower compared to that on the tubercle peak and trough. This means that there is a higher flow velocity over the flat leading edge, and thus potentially a higher lift coefficient.

6.4 Velocity Field

In Figure 48, 49 and 50 the velocity throughout the domain is presented as well as the velocity direction are plotted for the X- and Y- component. Observing these figures it is clear that the flow separation occurs later behind the tubercle compared to behind a trough and for the flat leading edge foil. The separation bubble is also smaller behind the tubercle compared to the other two cases.

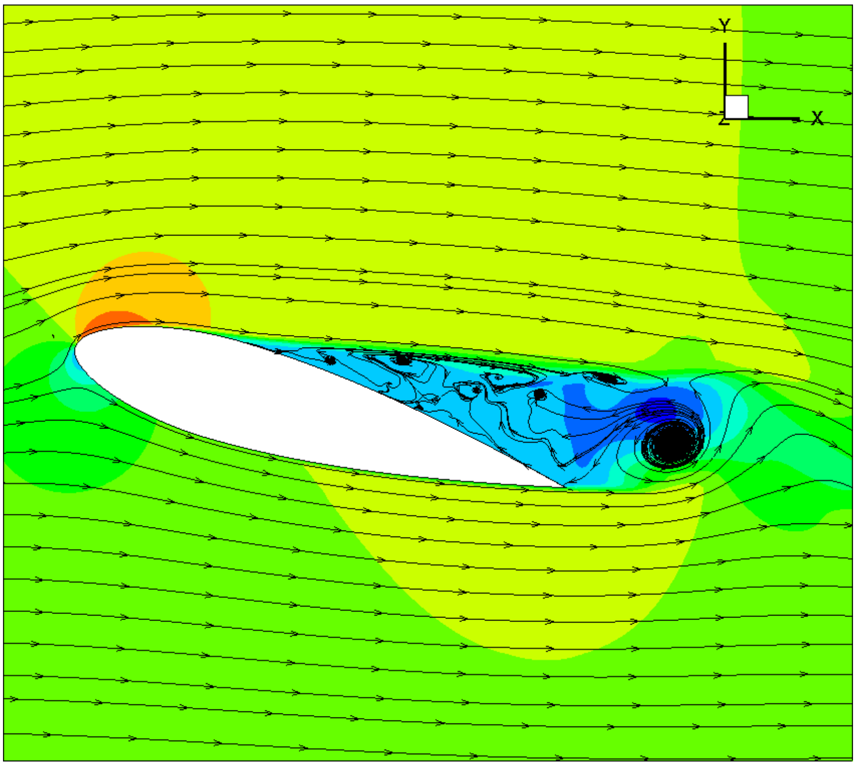

Figure 48: Vectorfield for Flat leading edge with AoA=16°.

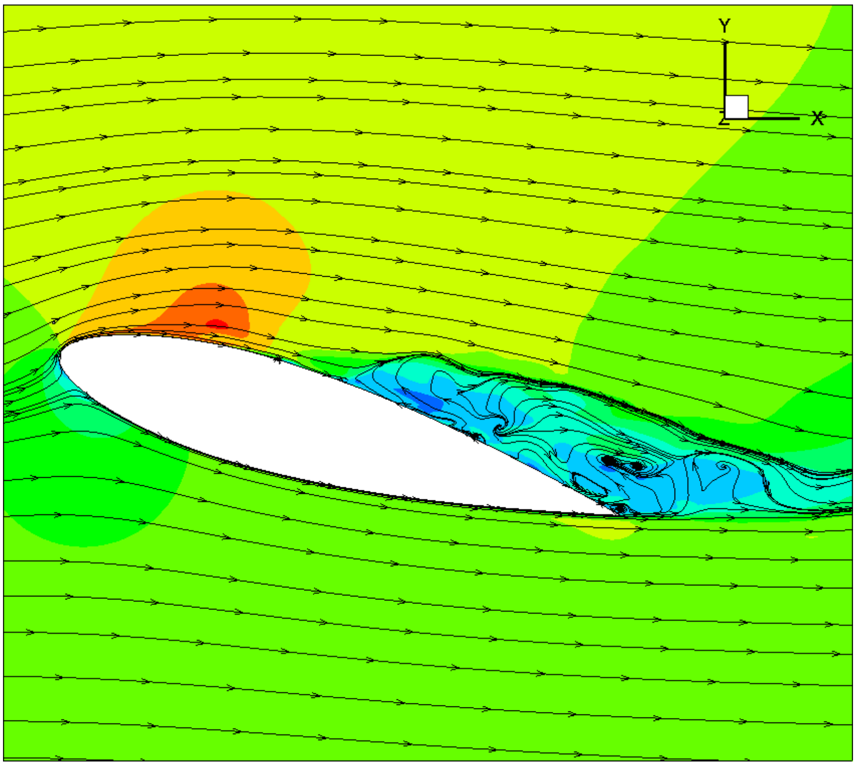

Figure 49: Vectorfield for A01N3 with AoA=16° at peak.

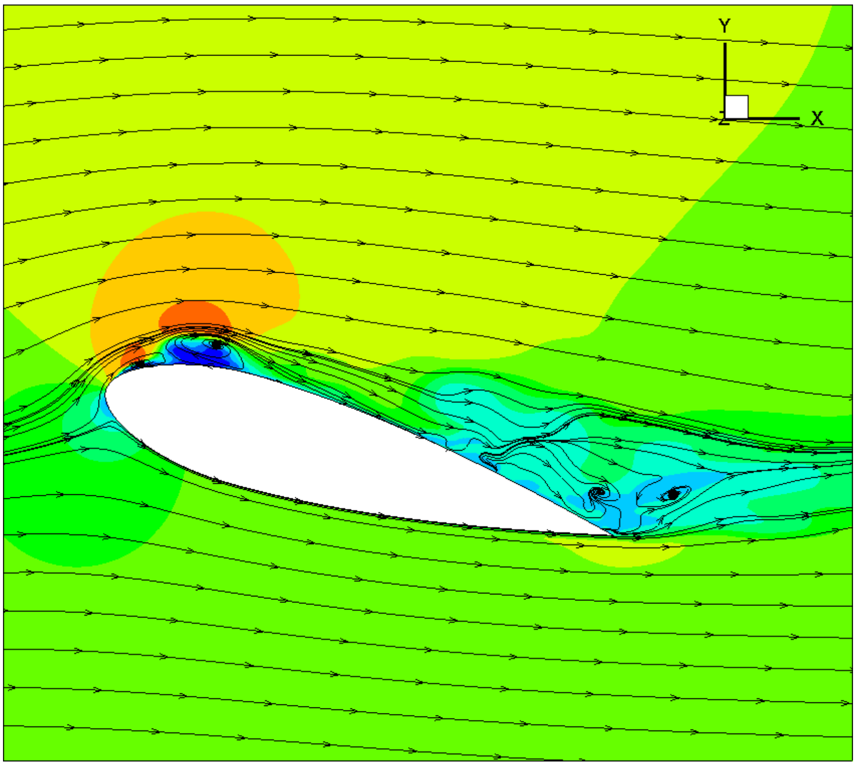

Figure 50: Vectorfield for A01N3 with AoA=16° at trough.

Figure 51 show the velocity in Y-direction along the span width. For the flat leading edge and tubercle foil A01N3. The velocity is measured at three different heights; 0.015 m, 0.010 m and 0.006 m above each foil. All three height levels are at 10% of the chord length from the leading edge. The velocity closest to the tubercle foil has at several points negative value which means that the flow structure created by the tubercles press down the flow on the foil surface. The interesting is that the flow velocity is negative at point 0.013, 0.04 and 0.067 in Z-direction. These points are all tubercle peak points. Although the flow are not at its lowest, the vortices still presses the flow down. This supports the theory that the vortexes generated by the tubercles press the fluid down towards the surface, and thus delaying separation.

However as predicted it also lifts the flow up away from the foil surface between the tubercles. Resulting in early separation for the flat foil, there is a negligible difference in velocity along the span width at the three different height levels. Thus a more stable flow over the leading edge occur.

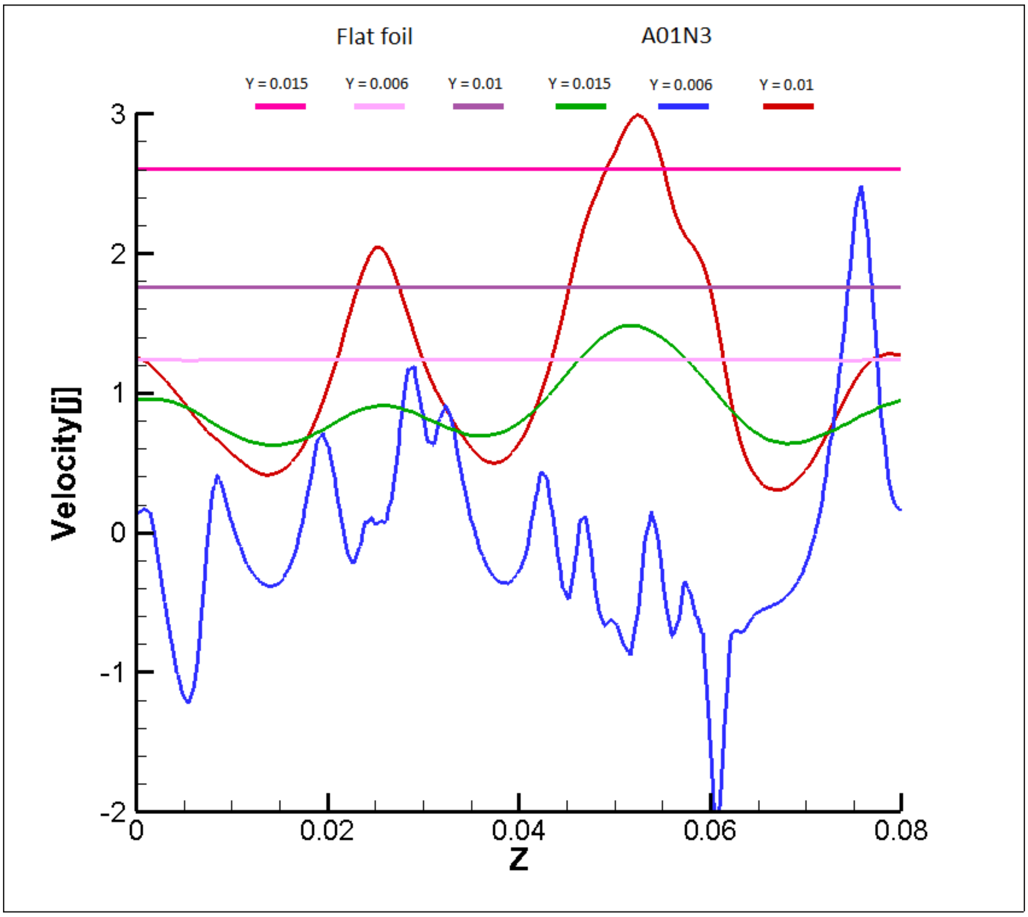

Figure 51: The velocity in Y-direction along the span at three different heights above the foil.

Figure 52 show the velocity in X-direction along the span width. As in Figure 51, a flat leading edge foil and foil A01N3. The measurements are done at the same heights and the same chord length as in figure 51.

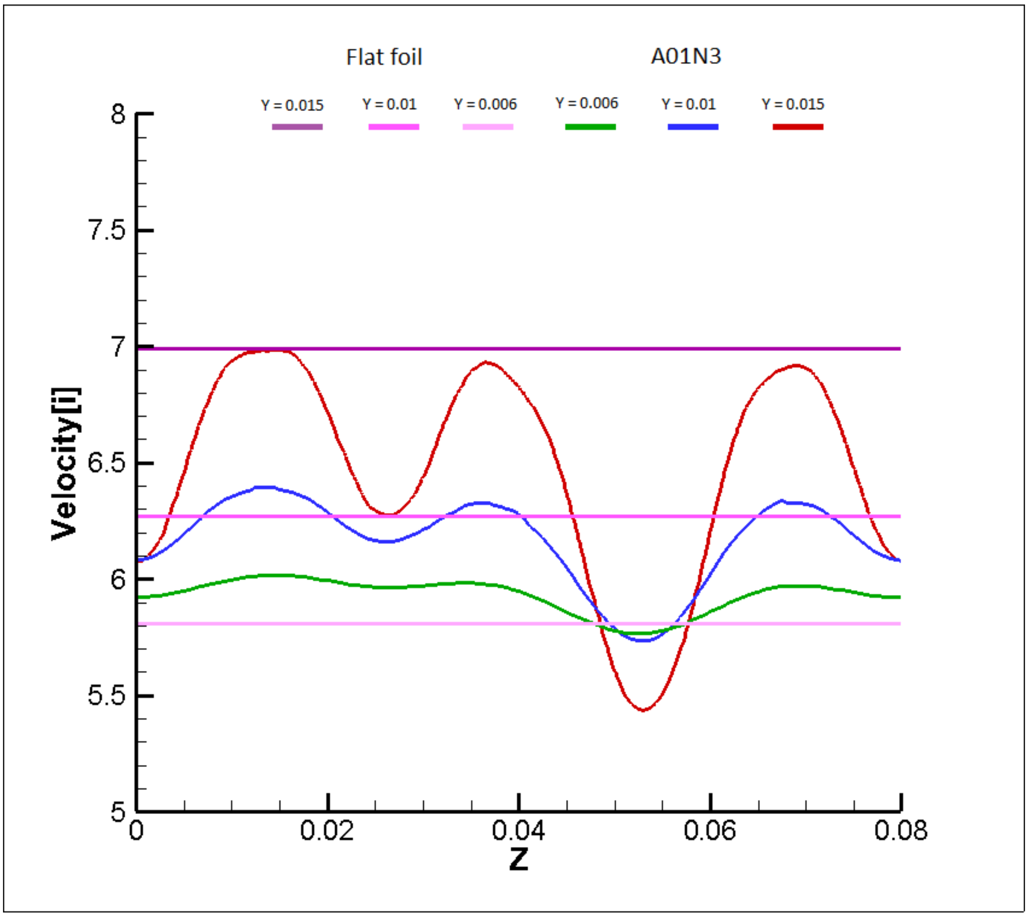

Figure 52: The velocity in X-direction along the span at three different heights above the foil.

The velocity in X-direction at Y=0.01 are of course less stable due to the presence of vorticies in the flow over the tubercle foil. However, it is in general lower than for the flat leading edge, except for at height Y = 0.006. The tubercle flow varies a lot due to the angular velocity induced by the tubercles.

The effect that was not predicted was how much the vorticies generated affected each other. The decrease in axial velocity at a trough in Z-direction at 0.055m can be seen in figure 52. However, the velocity is not equally low in any other tubercle trough which can be seen in figure 46e. The height of the slow moving flow at Z = 0.055 is much higher than for the other tubercles troughs, decreasing flow velocity all the way through the boundary layers.

7 Discussion

In this section the results will be discussed followed by different sources of error that could have occurred. Moreover recommendations on how the project should be continued will be presented.

7.1 Results

Based on several of the articles read in prior of this thesis, the project begun with the notion that the tubercles would increase the lift-to-drag ratio. Only one of the previous studies took a more sceptical stance (Hansen, 2012).

It is difficult to see a pattern between the lift-to-drag ratio and the characteristics of the foils investigated. The foil with tubercles yielding the highest lift-to-drag ratio, A002N2, have a low tubercle amplitude as well as few tubercles i.e long tubercle wavelength. This makes it quite similar to the flat foil in appearance. Also A005N21 which has a rather low amplitude but short wave length, making it similar to a flat foil yield a high lift-to-drag ratio. This may be why it has almost as high lift-to-drag ratio as the flat leading edge foil. The foils investigated which had the worst lift-to-drag ratio was the foils with a tubercle design where the tubercles have a high amplitude and the tubercles are a prominent part of the design.

In Figure 39 the lift coefficient for all foils investigated are plotted. This plot show several foils which have a higher lift coefficient at 16° compared to the flat leading edge. These foils are named A0075N5, A0075N3, A01N5,A01N3, A005N5 and A002N2. These foils, apart from A002N9, have tubercles which have a high amplitude and long wave length, i.e few tubercles. This means that the tubercle presence in the design is very clear and defined and it does not have any similarities to a flat leading edge foil. The foils with tubercle amplitude of 0.5% to 1% of the chord length yield a C_L around 0.9 while the flat leading edge foil produce a C_L of 0.7. A002N9 on the other hand, has a lower amplitude of 0.2%, and has a much shorter wavelength. This means that it is quite opposite of A01N3, but since the tubercle wavelength is quite short, the tubercles are still a significant and clear part of the leading edge design. The foils with low tubercle amplitude and short wavelength are the foils which have lower C_L than the flat leading edge foil. All these foils yield a lower C_L at 6° and 12° compared to a flat leading edge foil, which is not favourable.

The reason for the high lift coefficient for the foils with tubercles is believed to be due to the flow structure they create. Observing the vector field in Figure 49, 50 and 48, the flow separates later over the tubercle peak. This supports the theory investigation in section 3. The tubercles create vortices and thus increase the angular velocity in the flow. Not only does this increase the kinetic energy of the attached flow, thus increasing the momentum exchange, but it also presses the flow down towards the foil surface. This can be seen in Figure 51 where both flat leading edge foil and tubercle foil A01N3 is plotted. The plot shows the velocity in Y-direction in position 0.006m above the leading edge oscillating between positive and negative values. This means that at the points where the velocity is negative, the flow is pressed down towards the foil surface. Opposite to this, when the flow velocity is also positive the flow is pushed up away from the foil. This is not helpful in order to achieve late separated flow. When studying in the same plot, the flat leading edge foil, at all three height levels has a uniform velocity distribution in the spanwise direction. This meaning a more laminar flow.

The drag coefficient plot in Figure 40 tells another story than the lift coefficient plot in Figure 39. It show that every tubercle foil at every AoA, except A002N2, yields a higher drag coefficient compared to the flat leading edge foil. This result suggest then that tubercles are not beneficial but instead increase the resistance. Foil A002N2, which has a similar design to the flat leading edge foil, yields a lower drag coefficient compared to the flat leading edge foil. This indicates that low amplitude and high wave length might be beneficial for low drag coefficients.

When investigating the iso-surface plots in Figures 43a to 46g and the limiting streamlines in Figure 43 to 46 it can be seen that there are large areas with high levels of turbulent flow. Looking at the worst performing foil, A01N3, in Figure 46e, the flow oscillates much more than the flat leading edge foil in figure 43e. The limiting streamlines shown in Figure 46f and 46h show that the flow do separate early, thus inducing extra drag. One reason may be the decrease in velocity over the suction side in X-direction of the foil. Comparing Figure 43g and 46g, the velocity over the leading edge is approximately 2 m/s lower than on the leading edge of A01N3. As the flow changes from having only velocity in X-directon to having vecolity vectors in both X-,Y-, and in Z-direction, the velocity decreases. This may be one of the reason for the increase of drag generated by the flow.

What the CFD analysis also show is that the tubercles tend to affect each other in all limiting streamlines plots in Section 6.2. This can be seen for AoA=16° in Figure 45f, 46f, but occurs also at AoA=20°. The attached flow "splits" in two where the attached flow behind each tubercles is drawn to create two areas, one with no attached flow and one with attached flow. This was also seen by Rostamzadeh (Rostamzadeh et al., 2017) in his CFD results of the A2W7.5, and in the current validatio study in Section 5.2. Rostamzadeh concludes, as the authors of this thesis, that this separation bubble induced over the suction side results in lower lift coefficient and increased drag.

As mentioned before the tubercles on A002N2 do have a low amplitude and long wavelength. A002N2 has decreased drag, but while the flat foil has a C_L of 0.9, A002N2 only have a C_L of 0.57. The end result is a high lift-to-drag ratio compared to many other tubercle foils, but not good enough to claim that it is a better design than normal flat leading edge design.

Looking at Figure 39 illustrating C_L it can be seen that the foils with the highest value are not among those yielding the highest lift-to-drag ratio. Instead it is the foils with a good combination of a high C_L and a low C_D that yield the highest lift-to-drag ratio. The tubercle foils also have a lower lift-to-drag ratio at 6°. This could be a viable design if the tubercle foil had the same C_D as the flat leading edge. If the rudder generated high lift coefficients at high angles, the drag produced would not be significant problem since the vessel would still turn more rapid. However, when the rudder has increased drag at low AoA, where the rudder operates 90% of the time means more fuel and more power just to propel the vessel in a straight forward. Thus meaning the tubercle design is not beneficial.

7.2 Sources of error

There are several aspects in this project that have the risk of causing error. When handling great amounts of files for different simulations there is always a risk that there will be an error. With the validation studies and the present study having different values for the main particulars it is easy to forget to change the free stream velocity, giving a wrong Reynolds number as well as lift- and drag coefficient. Also the planform area is needed to calculate the lift- and drag coefficient, this has been changed manually for each simulation set up.

Furthermore have there have been a lot of different combinations of physical models, time steps and near wall mesh tested for the domain. There is always a risk that two results are compared to each other even if the values have been calculated in entirely different ways and with different values, disqualifying it from comparison.

To get a non-dimensional unit that can be compared between different foils, C_L and C_D have been used. When calculating these in accordance with equations 1 and 2. The expression for what the area indicates in the previous studies have not always been clear whereby guessing and reading between the rows have had to be done. For the project it was decided that the area should be expressed as a rectangle with the chord length multiplied with the span width i.e. the foil seen from straight above. A problem with this is that the planform area seen from above changes when an AoA is introduced. To be able to compare the data in a good and correct way the planform area for AoA=0° will be used for all AoA. This might be one of the reasons for the result being more accurate for low AoA where this wouldn't affect as much.

Another aspect that may have effected the result of the lift-to-drag ratio is the mesh size. There is always a conflict of interest between having a fine mesh, representing the surface correct, and having a coarse mesh reducing the computational time and the cost of simulating. This is especially important to take into account for the foils with a high number of tubercles where the decrease in size of the tubercle means that the mesh size need to decrease as well. For this project the amount of cells was compared to previous studies, having a similar domain and foil would give an indication of the amount of cells. After a domain set up giving the right amount of cells was found, the foil was inspected manually to confirm that the mesh represented the surface correct.

The foils with highest lift-to-drag ratio being the foils with the lowest tubercle amplitude supports the results from Hansen (2012). However, the lift-to-drag ratio for the foil with the lowest amplitude, A001N9, is not high. This raises questions of how much the amplitude affects the result, and if the results are enough to claim that a low amplitude is favourable. This may also be a question of the Reynolds number, if there is the Reynolds number where tubercle foils yields better result than the flat leading edge foil. This however, due to time limit, is for future work, but is a very valid factor which Hansen (2012) mentions in her conclusion.

7.3 Future Work

Further work with the project should include a deeper investigation of the lift-to-drag ratio for different amplitudes and waves length with a wider variety of combinations. It would be interesting to see how a change of the chord length would effect the lift-to-drag ratio and if the tubercles would be more beneficial for a different chord length.

All the different designs investigated have used the same tubercle design equation on all tubercles for each foil. Future work should investigated how the result would be effected by using different sizes of the tubercles on one foil. This could maybe help to increase the vortices pressuring down the flow and decrease those pushing the flow away from the foil.

Furthermore it would be good to run the simulations for a wider range of AoA, as it is now there are only four different AoA. To really be able to understand how the tubercles affect the lift-to-drag ratio further angles need to be investigated, especially for the critical angle of attack as well as for low AoA. Further simulations need to be conducted to see how the tubercles affect the drag for AoA=0°. With ships mostly having the rudder at a AoA=0° it can be beneficial to have more drag at high AoA if the lift is higher. This means that the ship would be more agile but at the same time need more power to the manoeuvring.

Moreover it would be interesting to run simulations with a range of different Reynolds number to see the effect of this. According to Hansen (2012) the most optimal range of Reynolds number were somewhere between 505,000-520,000 while Rostamzadeh et al. (2017) used Reynolds number 120,000 and 1,500,000. There is quite a difference in the magnitude between these numbers and further investigation for one specific foil at different AoA and different Reynolds numbers would be interesting.

8 Conclusion

The aim of this study was to investigate the effects on rudder efficiency by redesigning the leading edge of a rudder to mimic the leading edge of a humpback whales flipper.

During the study a domain for investigation and a parametric foil has been created. For the parametric foil the AoA, amplitude, thickness and wave length is easily varied. With these tools 16 different foils with tubercles on the leading edge and different AoA were designed. The foils were then transferred to STAR-CCM+ where simulations were conducted to see which foil that generated the highest lift-to-drag ratio.

Moreover a validation of three previously conducted studies has been made. This to ensure that the same result was obtained so that our study has facts to lean on.

The results show that the flat leading edge foil is the foil yielding the highest lift-to-drag ratio of all foils examined, contradicting earlier beliefs. Among the foils with tubercles it is the ones with a low amplitude and high wave length that give the highest lift-to-drag ratio. These foils look quite similar to the flat leading edge foil and that might be the reason for the similar performance as the flat leading edge foil.

However, looking at only the lift coefficient there are several foils yielding higher lift compared to the flat leading edge foil, especially those with tubercles with high amplitude and wave length. At the same time these foils produce a high drag coefficient, lowering the lift-to-drag ratio.

The present study can conclude that applying tubercles on the leading edge of a rudder could improve the maneuverability of a vessel but at the same time increase resistance. Most of the time vessels operate with the rudder at low AoA. If there is no change in drag for low AoA, for a foil with tubercles, it might be beneficial to accept higher drag for a high AoA if this means a higher lift which equals better maneuverability.

References

Amelia Hennighausen, Eric Roston (2017). *Inventions Inspired by Nature: Biomimicry.* URL: `https://www.bloomberg.com/news/photo-essays/2015-02-23/14-smart-inventions-inspired-by-nature-biomimicry` (visited on 02/23/2017).

Aokomoriuta (2011). *Law of the Wall.* URL: `https://commons.wikimedia.org/wiki/File:Law_of_the_wall_(English).svg` (visited on 05/01/2017).

Babinsky, Holger (2012). *How wings really work.* URL: `http://www.cam.ac.uk/research/news/how-wings-really-work` (visited on 05/11/2017).

Bakker, André (2006). *Lecture 11 – Boundary Layers and Separation.* URL: `http://www.bakker.org/dartmouth06/engs150/11-bl.pdf` (visited on 01/25/2017).

CCM+, Star (2017). *Star CCM+ User guide.* URL: `http://www.cfdyna.com/Notes/Solution/Segregated.pdf` (visited on 05/01/2017).

Colin, Cutler (2015). *How Does Aspect Ratio Affect Your Wing?* URL: `http://www.boldmethod.com/learn-to-fly/aircraft-systems/how-does-aspect-ratio-affect-a-wing/` (visited on 01/26/2017).

Fish, Frank and Juliann Battle (1995). "Hydrodynamic design of the humpback flipper". In: *Journal of Morphology* July.

Fish, Frank and Mark Murray (2011). "Marine Applications of the Biomimetic Humpback Whale Flipper". In: *Marine technology Society Journal Vol 45* July/August.

Fish, Frank, Paul Weber, et al. (2011). "The Tubercles on Humpback Whales' Flippers: Application of Bio-Inspired Technology". In: *Integrative and Comparative Biology* Volume 5.

Giraldo, F.X. (2006). *Hybrid eulerian-lagrangian semi-implicit time-integrators.* Vol. 52.

Hansen, Kristy Lee (2012). "Effect of Leading Edge Tubercles on Airfoil Performance". PhD thesis.

Hoffman, Gregorek M. and Berchak (1989). "Steady State and Oscillatory Aerodynamic Characteristics of a NACA0021 Airfoil: Data Report". In:

Jab, Frozee (2015). *Construction and Types of Rudder on Ships.* URL: `http://marineengineeringonline.com/construction-and-types-of-bearing-on-ships/` (visited on 01/24/2017).

Jay, Moran (2016). *How To Build High a Performance Rudder.* URL: `http://www.paceship.org/how_to/rudder.asp#theory` (visited on 01/24/2017).

Lohry, Mark et al. (2012). "Characterization and Design of Tubercles Leading-Edge Wings". In: *International Conference on CFD* 7th.

Marzocca, Pier (2017). *The NACA airfoil series*. URL: http://people.clarkson.edu/~pmarzocc/AE429/The%20NACA%20airfoil%20series.pdf (visited on 02/07/2017).

Menter, Florian M. (1994). "Zonal Two Equation k-omega Turbulence Models for Aerodynamic Flows". In: *AIAA Journal* 32.8.

Nierop, Ernst A. van et al. (2009). "How Bumps on Whale Flippers Delay Stall: An Aerodynamic Model". In: *Physical Review Letters* February.

Rostamzadeh, Nikan et al. (2017). "A numerical investigation inteo the effect of Reynolds number on the flow mechanism induced by a tubercled leading edge". In: *Theoretical Computional Fluid Dynamics* 31.

Science, Flow (2017). *Implicit Vs. Explicit Numerical Methods*. URL: https://www.flow3d.com/resources/cfd-101/numerical-issues/implicit-versus-explicit-numerical-methods/ (visited on 05/01/2017).

Shi, Weichao et al. (2016). "Numerical optimization and experimental validation for a tidal turbine blade with leading-egde tubercles". In: *Elsevier* Renewable Energy 96(October).

Soumya, Chakraborty (2016). *How Does A Rudder Help In Turning A Ship?* URL: http://www.marineinsight.com/naval-architecture/rudder-ship-turning/ (visited on 01/24/2017).

Spalart, P.R. and S.R. Allmaras (1994). "A one-equation model Turbulence Model for Aerodynamic flows". In: *La Rechere Aérospatiale* 1.

Stanway, Michael Jordan (2008). *Hydrodynamic effects on the leading-edge tubercles on control surface and in flapping foil propulsion*. Tech. rep. Massachusetts Institution of Technology.

Strelets, M. (2001). "Detached Eddy Simulation of Massively Separated Flows". In: *Aerospace Sciences Meeting and Exhibit* 39th.

Team, LEAP CFD (2012). *Turbulence Part 2 - Wall Functions and Y+ requirements*. URL: https://www.computationalfluiddynamics.com.au/tips-tricks-turbulence-wall-functions-and-y-requirements/ (visited on 02/14/2017).

– (2013). *Turbulence Part 3 - Selection of wall functions and Y+ to best capture the Turbulent Boundary Layer*. URL: https://www.computationalfluiddynamics.com.au/turbulence-part-3-selection-of-wall-functions-and-y-to-best-capture-the-turbulent-boundary-layer/ (visited on 02/14/2017).

Vacanti, David (2005). "Keel and Rudder Design". In: *Proffesional BoatBuilder* June/July.

Weber, Paul, Laurens Howle, et al. (2010). "Lift, Drag, and Cavitation Onset On Rudder With Leading-Edge Tubercles". In: *Marine technology Vol 47* January.

Weber, Paul, Howle Laurens, et al. (2011). "Computational Evaluation of the Performance of Lifting Surfaces with Leading-Edge Protuberances". In: *Journal of Aircraft* Volume 48.2.

White, Frank M. (2011). *Fluid Mechanics*. 7th edition. McGraw-Hill. Chap. 7.4 Flat-Plate Boundary Layer.

Zhiyin, Yang (2015). "Large-eddy simulation: Past, present and the future". In: *Chinese Journal of Aeronautics* 28.

A Appendix

A.1 Models used in STAR-CCM+

A.1.1 Mesh Modelling

- Trimmer
- Surface Remesher
- Prism Layer Mesher

A.1.2 Physic Modelling

- All y+ wall distance
- Constant Density
- Exact Wall Distance
- Gradients
- Three Dimensional
- Turbulent
- Segregated Flow
- Detached Eddy Simulation
- Spalart-Allmaras Detached Eddy